Title

An epoxide hydrolase inhibitor reduces neuroinflammation in a mouse model of Alzheimer's disease

Journal

Science Translational Medicine, 12(573)

ISSN

1946-6234

Authors

Ghosh, Anamitra

Comerota, Michele M

Wan, Debin

et al.

Publication Date

2020-12-09

DOI

10.1126/scitranslmed.abb1206

Peer reviewed

Published in final edited form as:

Sci Transl Med. 2020 December 09; 12(573): . doi:10.1126/scitranslmed.abb1206.

An epoxide hydrolase inhibitor reduces neuroinflammation in a mouse model of Alzheimer's disease

Anamitra Ghosh[1], **Michele M. Comerota**[1], **Debin Wan**[2], **Fading Chen**[1], **Nicholas E. Propson**[1,3], **Sung Hee Hwang**[2], **Bruce D. Hammock**[2], **Hui Zheng**[1,3,4,*]

[1]Huffington Center on Aging, Baylor College of Medicine, Houston, TX

[2]Department of Entomology and Nematology and UCDMC Comprehensive Cancer Center, University of California, Davis, CA

[3]Department of Molecular and Cellular Biology, Baylor College of Medicine, Houston, TX

[4]Department of Molecular and Human Genetics, Baylor College of Medicine, Houston, TX

Abstract

Neuroinflammation has been increasingly recognized to play a critical role in Alzheimer's disease (AD). The epoxy fatty acids (EpFAs) are derivatives of the arachidonic acid metabolism pathway and have anti-inflammatory activities. However, their efficacy is limited due to their rapid hydrolysis by the soluble epoxide hydrolase (sEH). We report that sEH is predominantly expressed in astrocytes and its concentrations are elevated in postmortem brain tissue from AD patients and in the 5xFAD β-amyloid mouse model of AD. The amount of sEH expressed in AD mouse brains correlated with a reduction in brain EpFA concentrations. Using a specific small molecule sEH inhibitor, 1-trifluoromethoxyphenyl-3-(1-propionylpiperidin-4-yl) urea (TPPU), we report that TPPU treatment protected AD mice against LPS-induced inflammation in vivo. Long-term administration of TPPU to the 5xFAD mouse model via drinking water reversed microglia and astrocyte reactivity and immune pathway dysregulation. This was associated with reduced β-amyloid pathology and improved synaptic integrity and cognitive function on two behavioral tests. Importantly, TPPU treatment correlated with an increase in EpFA concentrations in the brains of 5xFAD mice, demonstrating brain penetration and target engagement. These findings support further investigation of TPPU as a potential therapeutic agent for the treatment of AD.

One Sentence Summary:

*To whom correspondence should be addressed: Hui Zheng, huiz@bcm.edu.

Author Contributions: AG and HZ designed the overall study. AG performed all in vitro and in vivo assays and associated biochemical and immunohistochemical experiments as well as data analysis, with technical assistance from MC and NEP. MC and FC performed mouse behavioral tests and LTP recordings and associated data analysis, respectively. SHH and BDH provided TPPU and advised on the related experiments. DW performed mass spectrometry analysis of oxylipins. AG and HZ wrote the manuscript and all authors read, provided input and approved the manuscript.

Competing interests: S.H.H. is a part-time employee and B.D.H. is a cofounder and CEO of EicOsis LLC. H.Z. is on the Scientific Advisory Board of the Tau Consortium managed by the Rainwater Charitable Foundation.

Data and materials availability: All data associated with this study are present in the paper or the Supplementary Materials. Gene expression data have been deposited in NCBI with GEO accession number GSE161848. TPPU and EC5026 are commercially available from Cayman (MI, USA) and MedChemExpress (NJ, USA), respectively.

Blocking epoxide hydrolase with a bioavailable small molecule inhibitor reduces neuropathology in an Alzheimer's disease mouse model.

Accessible Summary:

Neuroinflammation is strongly implicated in Alzheimer's disease (AD). The epoxy lipids produced from arachidonic acid have anti-inflammatory properties, but they are rapidly turned over by the soluble epoxide hydrolase (sEH). We found that sEH is elevated in the brain of AD patients and an amyloid mouse model, suggesting that blocking sEH may replenish the epoxy lipids and combat neuroinflammation. Indeed, treating the amyloid mice with a small molecule sEH inhibitor restored the epoxy lipids, reduced neuroinflammation and amyloid pathology, and improved cognition. Our study identifies a lipid metabolic pathway regulating neuroinflammation and provides support for sEH inhibitors as AD therapy.

Introduction

Alzheimer's disease (AD) is the most common form of age-associated neurodegenerative disorder pathologically defined by the deposition of extracellular beta amyloid (Aβ) plaques and the accumulation of intracellular neurofibrillary tangles (1). Overwhelming evidence supports a crucial role of Aβ in initiating a cascade of pathogenic events leading to cognitive impairment and neurodegeneration (2, 3). Hence, the majority of AD clinical trials have been focused on Aβ. Unfortunately, these trials have been unsuccessful so far (2, 4–6). Thus, there is an urgent need to pursue other disease modifying therapies.

Besides the pathological hallmarks, AD is associated with prominent neuroinflammation (7, 8). Prolonged activation of glial cells, microglia and astrocytes in particular, and the release of proinflammatory cytokines, chemokines, and reactive oxygen and nitrogen species, create a neurotoxic environment which could exacerbate the progression of AD (9–11). Recent genomewide association studies identified multiple immune related gene variants as risk factors for late-onset AD, supporting a major contributing role of innate immunity and neuroinflammation in AD (12–15). However, while epidemiological studies indicated positive effects of nonsteroidal anti-inflammatory drugs (NSAIDs) such as cyclooxygenase (COX) inhibitors in AD protection, randomized clinical trials failed to demonstrate clinical efficacy (16, 17).

COX, along with lipoxygenase (LOX) and cytochrome P450 monooxygenase (CYP), belong to the arachidonic acid metabolic pathway that produces prostaglandins, leukotrienes, and various epoxy fatty acids (EpFAs) including epoxyeicosatrienoic acids (EETs) and epoxy-docosapentaenoic acids (EDPs) from arachidonic acid, respectively (fig.S1A 1A) (18, 19). Among these, the COX and LOX pathways have been extensively studied and successfully targeted therapeutically (18). In contrast, much less is known about the therapeutic potential of targeting the CYP pathway.

EETs and EDPs have been demonstrated to possess anti-inflammatory and neuroprotective properties through multiple mechanisms. EETs inhibit VCAM-1, E-selectin and ICAM-1 expression in endothelial cells to block monocyte infiltration (20). By inhibiting NF-κB

nuclear translocation, EpFAs downregulate several proinflammatory molecules including the inducible nitric oxide (iNOS) and COX-2 (20–22). Further, EETS and EDPs have been shown to reduce inflammation and neurodegeneration by acting on signal transducer and activator of transcription 3 (STAT3) and nuclear hormone receptors such as peroxisome proliferator activated receptor (PPAR) alpha and gamma (23, 24). However, EpFAs are broken down rapidly into corresponding diols by the soluble epoxide hydrolase (sEH). sEH, encoded by the *EPHX2* gene, contains a N-terminal phosphatase and C-terminal hydrolase domain and exists as a homodimer (25). sEH is widely expressed in both peripheral tissues and the central nervous system (CNS). Elevated sEH expression has been reported in CNS disorders such as depression (26), schizophrenia (27), Parkinson's disease (28), and recently AD (29, 30). sEH inhibition by genetic deletion or pharmacological blockade has been shown to confer beneficial effects in mouse models of these diseases, but few mechanistic insights have been provided. Importantly, whether these effects are associated with changes in EpFAs remains unclear.

Here, we present evidence that sEH is aberrantly elevated in postmortem brain tissue from AD patients and in APP/Aβ transgenic and knock-in mouse models of AD. Using a selective sEH inhibitor, 1-trifluoromethoxyphenyl-3-(1-propionylpiperidin-4-yl) urea (TPPU) that specifically inhibits the C-terminal hydrolase activity of the sEH (26, 31), we demonstrate that long-term administration of TPPU to the 5xFAD mouse model of AD restored EpFA concentrations and reversed microglia and astrocyte reactivity in mouse brain. These changes were accompanied by attenuated β–amyloid pathology and improved synaptic integrity and cognitive function in the AD mouse brain.

Results

Elevated sEH and diminished EpFA in postmortem mouse and human brains

Arachidonic acid is an omega-6 unsaturated fatty acid released from the membrane phospholipids by phospholipase A2 (PLA_2) or derived from endocannabinoids by fatty acid amide hydrolase (FAAH), and can be further metabolized by COX, LOX or CYP (fig. S1A) 1A) (32). We first evaluated the expression of arachidonic acid metabolic pathway genes in postmortem AD brain samples and age-matched controls without dementia. Quantitative real-time PCR (qPCR) analysis showed that the expression of *PLA2G2A*, but not *FAAH*, was elevated in postmortem AD human brains (fig. S1B), suggesting that PLA2-mediated release, but not endocannabinoid conversion, may be a driver for changes in arachidonic acid metabolism in AD. Expression of both the *COX2* and *CYP4F8* genes, which produce prostaglandin and its metabolite PGE_2, respectively, was increased suggesting overall activation of the COX pathway. Interestingly, examination of the CYP monooxygenase pathway revealed that, whereas no differences in several of the CYPs, including *CYP2J2*, *CYP2C8* and *CYP2C19*, were detected, expression of *EPHX2* was higher in AD postmortem brain samples compared to control brain samples (fig. S1B).

Consistent with the mRNA expression, Western blot analysis revealed a nearly two-fold increase of sEH protein in postmortem AD brains compared to control brains (Fig. 1, A, B). Elevated *Ephx2* mRNA (Fig. 1C) and sEH protein (Fig. 1, D and E) were also detected in the cortex and hippocampus of 5xFAD transgenic mice at 4.5 months of age compared to

their littermate non-transgenic controls. This result was further validated in an APP^{NLGF} knock-in mouse model of AD with physiological expression of APP (33) (fig. S1, C–D). Consistent with elevated sEH, lipodomics analysis of two major sEH EpFA substrates, EETs and epoxydocosapentaenoic acids (EDPs), by LC-MS/MS showed a reduction in multiple EET and EDP regioisomers in transgenic mouse brains in comparison to nontransgenic control mouse brains (Fig. 1F). Thus, heightened sEH expression was a common feature in human AD and APP/Aβ mouse brain samples, which in 5xFAD mice resulted in reduced EpFA.

TPPU and EETs block astroglial sEH upregulation and LPS-induced inflammation in vitro

To assess the cell type expression of sEH, we used a flow cytometry-based concurrent brain cell type acquisition (CoBrA) method to simultaneously isolate astrocytes, microglia and vascular endothelial cells from 4.5 month-old non transgenic control and transgenic 5xFAD mouse brains (34). qPCR analysis revealed that *Ephx2* was highly expressed in sorted astrocytes and that expression was higher in transgenic compared to nontransgenic mice (Fig. 2A). In contrast, *Ephx2* expression was lower in microglia and endothelial cells and no significant differences were detected between transgenic and nontransgenic mouse brain samples. This result was substantiated by co-immunofluorescence staining for sEH and astrocyte (GFAP) or microglia (Iba-1) markers in hippocampal sections of nontransgenic and transgenic mouse brains (Fig. 2B). We observed elevated expression of sEH predominantly in GFAP-positive astrocytes in transgenic mouse brain samples, with negligible co-staining with Iba1. Both the sEH fluorescence intensity and the number of sEH expressing cells were increased in transgenic AD compared to nontransgenic control mouse brains (Fig. 2C). Similar astrocytic upregulation of sEH was also observed by acute LPS administration in vivo (fig.S2) and in primary astrocyte cultures (fig. S3, A and B). Next, we tested the effect of the sEH inhibitor TPPU in LPS-treated mouse primary astrocyte cultures. Thirty minutes treatment with TPPU dose-dependently reduced nitrite release as measured by the Griess assay (Fig. 2D), and reduced the expression of proinflammatory molecules *Il-1α*, *Il-1β*, *Tnf-α*, *Il-6*, *iNOS* and *Gfap* (Fig. 2E) and *Ccl-2* and *Cxcl-1* (fig. S3C). The reduced expression of iNOS and GFAP were confirmed by immunostaining (Fig. 2, F and G).

Next, we wondered whether the anti-inflammatory effect of sEH inhibition could be attributed to increased EETs. Although a membrane receptor for EET has yet to be identified, epoxyeicosa-5(Z)-enoic acid (EEZE) has been reported to act as a direct EET antagonist on the cell membrane or intracellularly (35) where it blocks the vascular actions of the EETs (36, 37) and the anti-inflammatory effect of the sEH inhibitor adamantane-1-yl-ureido]-dodecanoic acid (AUDA) in cultured microglia (38). We thus tested the effect of EEZE by pre-treating the primary astrocytes with TPPU or 14,15-EEZE 30 minutes prior to LPS treatment and measuring nitrite release by the Griess assay. The inhibitory effect of TPPU was completely abolished upon co-treatment with 14,15-EEZE (Fig. 2H), suggesting that EETs may be the functional mediators of TPPU. Supporting this assessment, 30-minute pre-treatment of mouse primary astrocyte cultures with 11,12-EET attenuated LPS-induced nitrite release in a dose-dependent manner (Fig. 2I).

In agreement with the astroglial specific expression of sEH, TPPU had no effect on LPS-treated mouse primary microglia cultures measured by the expression of pro-inflammatory molecules (Fig. 3A) or iNOS induction (Fig. 3B, C). However, when the same treatment was applied to mixed mouse astrocyte and microglia cultures, TPPU attenuated iNOS production in both cell types (Fig. 3, D and E) and reduced cytokine expression (Fig. 3F), suggesting that TPPU may act on astrocytes to suppress microglial reactivity through secreted EETs. Indeed, direct EET treatment of mouse primary microglia monocultures also blocked LPS-induced reactive nitrogen species (Fig. 3G) and the expression of the pro-inflammatory molecules *Il-1α*, *Il-1β*, *Tnf-α*, *Il-6*, *iNOS* and *C3* (fig. S4). The efficacy of EET in preventing LPS-induced cytokine expression was further validated using an ex vivo mouse hippocampal organotypic slice culture system (fig. S5). Collectively, these results support a mechanism whereby TPPU inhibited astroglial sEH activity, and the resulting augmentation of EETs exerted anti-inflammatory effects in both astrocytes and microglia through autocrine and paracrine activities.

TPPU mitigates LPS-induced acute inflammation in vivo

Given the anti-inflammatory effects of TPPU in vitro, we next assessed its in vivo efficacy. We first examined whether TPPU is a substrate for P-glycoprotein, which mediates the ATP-dependent efflux of drugs or xenobiotics (39). Using the well-established human Caco-2 cell line (40, 41), we determined that the apparent permeability coefficient (P_{app}) for TPPU from the basolateral to the apical surface of Caco-2 cells in culture was 24.45×10^{-6} cm/s and from apical to basolateral surface was 18.03×10^{-6} cm/s (Table S1). Thus, the overall efflux ratio was 1.36, which was decreased to 0.99 in the presence of verapamil, a P-glycoprotein inhibitor. Given that a ratio of >2 is generally considered to involve P-glycoprotein-mediated efflux (41), TPPU is unlikely to be a favorable P-glycoprotein substrate.

Next, we investigated the effect of TPPU in LPS-induced inflammation by first treating C57BL/6 mice with TPPU (3 mg/kg) via oral gavage for 24 hours, and then followed by co-treatment with LPS (3 mg/kg, i.p.) and TPPU (3 mg/kg, oral gavage) for 18 hours (fig. S6A). Consistent with the in vitro and ex vivo studies, qPCR analysis of mouse brain samples showed that LPS triggered the expression of proinflammatory molecules in both the cortex and hippocampus, the majority of which were reduced by TPPU (fig. S6B). Western blotting showed that expression of iNOS, COX-2, GFAP, Iba-1 and sEH were upregulated in LPS-treated mice but downregulated by TPPU in both the hippocampus and cortex (fig. S6, C–F). Immunofluorescence staining of Iba-1 and GFAP and co-staining with COX-2 and iNOS documented that TPPU treatment mitigated LPS-induced microglia and astrocyte staining intensities as well as COX-2 and iNOS immunoreactivities (fig. S7). The anti-inflammatory effect of sEH antagonism was further validated using another sEH inhibitor EC5026 (fig. S8). Together, the results suggest that sEH blockade by TPPU may prevent acute neuroinflammation in vitro and in vivo.

TPPU enters the brain and engages its target under chronic treatment conditions in mice

Given the heightened expression of sEH in AD postmortem human brains and mouse models and the acute anti-inflammatory effect of TPPU, we next tested the long-term effect of TPPU in the 5xFAD transgenic mouse model of AD. We chose to start the treatment at 2

months of age as increased *Ephx2* expression was detected at this age and remained relatively stable for up to 15 months (fig. S9). We supplied either Vehicle or TPPU to transgenic AD mice and their nontransgenic littermate controls via drinking water continuously for 2.5 or 4.5 months (fig. S10A). Measurement of average water consumption per week per mouse for 10 weeks found no significant differences between the vehicle-treated and TPPU-treated transgenic mouse groups, demonstrating that TPPU did not affect fluid intake (fig. S10B). Measurement of TPPU in brain and plasma samples showed that, whereas TPPU was undetectable in vehicle-treated control brain and plasma samples, its concentration could be measured in the brain (fig. S10C) and plasma of treated mice (fig. S10D). The resulting brain to plasma ratio was 21.7% and 17.2% for the nontransgenic and transgenic mouse groups, respectively, similar to the ratio reported by acute administration (26). These results establish that TPPU was able to gain access to the mouse brain where its concentration could be maintained under chronic treatment conditions.

To determine the target engagement of TPPU in the mouse brain, we measured the concentration of EETs and EDPs, which were reduced in 5xFAD transgenic mouse brains (Fig. 1F). We found that the EETs (Fig. 4A) and EDPs (Fig. 4B) were elevated in TPPU-treated transgenic mice compared to the vehicle-treated control transgenic mouse group. The trending, but not statistically significant, increases of some of the regioisomers of EETs and EDPs could be attributed to the differences in drug uptake or responses among individual animals. Interestingly, plotting the co-expression relationship between EpFA regioisomers and TPPU indicated positive correlations between these two factors in the brain (Fig. 4C, D), strengthening the notion that TPPU penetrated the mouse brain and antagonized its target sEH.

TPPU treatment reverses immune pathway dysregulation in transgenic mice

Having established the efficacy of TPPU, we tested its effects in 5xFAD mice using molecular, biochemical, neuropathological and functional approaches (fig. S10A). To investigate the molecular mechanisms, we performed multiplex gene expression analysis using a Nanostring nCounter panel enriched for inflammatory genes. We quantified expression of 757 genes in the hippocampi of 4.5-month-old nontransgenic and transgenic mice treated with vehicle or TPPU (n=4/group). A volcano plot representation of gene expression stratified by vehicle-treated transgenic versus nontransgenic mouse groups (Fig. 4E) demonstrated upregulation of 171 genes (red dots) in transgenic mice. For each dot, significance was plotted against fold-change (log2 values). Treatment with TPPU for 2.5 months resulted in downregulation of 73 inflammatory genes (blue dots) in the treated compared to the untreated transgenic mouse group (Fig. 4F). Heatmap analysis of the 73-gene inflammatory group for individual animals demonstrated that increased inflammatory gene expression was downregulated by TPPU compared to vehicle-treated transgenic mice (Fig. 4G). Next, we performed gene ontology (GO) enrichment analysis to gain further insights into the biological functions of differentially expressed genes. Our results showed that 64 pathways were significantly enriched for the identified differentially expressed genes ($P < 0.05$) (Fig. 4H). Differentially expressed genes between transgenic and non transgenic mice were mainly enriched in immune-related processes, such as immune responses, inflammatory responses, chemokine responses, cytokine mediated signaling, the iNOS

biosynthetic pathway, the complement activation pathway, LPS-mediated signaling pathway, cell adhesion and chemotaxis pathways, NF-κB mediated signaling and apoptotic signaling pathways (Fig. 4H). All The majority of the inflammatory pathways upregulated in vehicle-treated transgenic mice were downregulated after TPPU treatment of transgenic mice (Fig. 4H). The Nanostring nCounter panel results were further validated by qPCR analysis of selected proinflammatory molecules using both cortex and hippocampal tissues obtained from transgenic mice treated with vehicle or TPPU (Fig. 4I).

In line with the gene expression data, Western blot analysis documented elevated inflammatory markers (iNOS and COX-2) and glial cell (GFAP and Iba-1) markers in the brains of 5xFAD transgenic mice compared to nontransgenic control animals in both hippocampus (Fig. 5A, B) and cortex (fig. S11). 2.5 months of TPPU treatment resulted in downregulation of these marker proteins (Fig. 5A, B and fig. S11), as well as p38 MAP kinase activation previously shown to be subject to regulation by EET (42). These results were further validated by immunofluorescence staining of Iba-1 (Fig. 5C) and GFAP (Fig. 5D) and co-staining with COX-2 and iNOS, followed by quantification (Fig. 5E). Together, the findings suggest that inhibition of sEH by TPPU was effective at reversing the dysregulated immune pathways and glia reactivity in 5x FAD transgenic mice.

TPPU ameliorates Aβ pathology and functional impairment

Having demonstrated a potential role for TPPU in reversing AD-associated immune system dysfunction, we then asked whether sEH inhibition by TPPU could influence Aβ pathology. We stained brain sections from 4.5 month old and 6.5 month old 5xFAD transgenic mice treated with vehicle or TPPU with the 6E10 antibody that recognizes the first 16 amino acid of the Aβ sequence and quantified Aβ plaque pathology in the hippocampus (Fig. 6) and cortex (fig. S12). We observed modest 6E10-positive Aβ plaque deposition in 4.5 month old 5xFAD transgenic mice treated with vehicle (Fig. 6A), which became more severe at 6.5 months of age (Fig. 6C). TPPU treatment led to reductions in the number and size of Aβ plaques and in 6E10 antibody staining intensity in both the 4.5 month (Fig. 6B) and the 6.5 month (Fig. 6D) age groups. Characterization of glial cells surrounding the plaques using general astrocyte (GFAP) and microglia (Iba-1) markers, as well as a phagocytic microglia marker (CD68) and a neurodegenerative glia marker (MGnD) (43), revealed reduced numbers of microglia per Aβ plaque (Fig. 6E, F). These changes could have been due to reductions in amyloid plaque size as the ratio of GFAP/6E10 or Iba-1/6E10 staining intensities were comparable between vehicle-treated and TPPU-treated groups (fig. S12A). Similar results were obtained when 4.5 month old mouse cortical samples (fig. S12B,C) or 6.5 month old mouse hippocampal samples (fig. S13) were analyzed.

To address whether the reduced Aβ pathology may have been caused by a possible off-target effect of TPPU on APP processing and Aβ metabolism, we performed biochemical characterizations of APP and APP processing enzymes, including BACE1 and the μ-secretase complex (composed of Nicastrin, PEN2, PS1 or PS2) (Fig. 6G). Two APP antibodies were used: the human-specific 6E10 antibody (hAPP) and a C-terminal antibody that recognizes both mouse and human full-length APP (APP-FL) and the APP C-terminal fragment (CTF). No appreciable differences were detected between vehicle-treated and

TPPU-treated 5xFAD transgenic mouse groups (Fig. 6H). The same results were obtained by qPCR analysis of *App*, *Adam10* and the Aβ degrading enzymes *Ide* and *Klk7* in both the mouse cortex and hippocampus (fig. S14). These results argued against an off-target effect of TPPU.

Having demonstrated a prominent role of TPPU in attenuating neuroinflammation and amyloid pathology, we next assessed the brain neuronal phenotypes following long-term TPPU treatment. We chose 6.5-month-old 5xFAD transgenic mice with 4.5 months of TPPU treatment for analysis as synapse and neuronal loss could be readily detected in these mice at that age (44–47). Co-immunostaining of the presynaptic protein synaptophysin with the neuronal marker NeuN and comparison of nontransgenic or transgenic mice treated with vehicle or TPPU revealed reduced synaptophysin intensity in area CA3 of the hippocampus in transgenic mice compared to nontransgenic controls (Fig. 7A, B). TPPU treatment partially elevated synaptophysin expression in transgenic mouse brains compared to the brains of mice treated with vehicle control (Fig. 7A, B). Double immunostaining for synaptophysin and postsynaptic protein PSD95 followed by high resolution imaging and quantification showed diminished synaptophysin/PSD95 positive synaptic puncta in 5x FAD mice, which was rescued by TPPU treatment (Fig. 7C,D). Measurement of NeuN-positive neurons in different brain areas including the subiculum, layer V of cortex and hippocampal CA3 region all showed different degrees of neuronal loss in the 5xFAD transgenic mice and partial rescue by TPPU treatment (Fig. 7E and fig. S15A). Expression of neuronal and synaptic markers correlated with synaptic plasticity measured by LTP recordings of the Schaffer collateral pathway of the hippocampus (Fig. 7F, G).

Interestingly, synaptophysin and NeuN double immunostaining of brain sections from 4.5 month old 5xFAD transgenic mice revealed that reduced synaptophysin immunoreactivity was observed at this age even though the number of NeuN-positive neurons remained unchanged (fig. S15, B–D). Given that increased synaptophysin staining intensity could be detected after TPPU treatment (fig. S15C), we wondered whether this was associated with functional improvement at this age. We thus evaluated the effect of TPPU treatment on cognition using the novel object recognition test (Fig. 7H) and a fear conditioning paradigm (Fig. 7I). The novel object recognition test assesses the hippocampus-dependent long-term recognition memory by calculating the percent time spent with a novel object (object discrimination index, ODI). The vehicle-treated 5xFAD mice displayed a decreased ODI average, which was elevated upon TPPU treatment (Fig. 7H). We further performed fear conditioning to test hippocampal dependent (contextual test) and independent (cued test) associative learning (Fig. 7I). The four groups tested exhibited no differences in freezing percentage during the conditioning phase. During the context test, vehicle-treated 5xFAD transgenic mice displayed a decreased freezing percentage compared to nontransgenic mouse groups, suggesting an impaired contextual memory. Comparatively, the TPPU-treated 5xFAD transgenic mice exhibited an increase in freezing frequency compared to the vehicle-treated transgenic mouse group. In addition, the percentage of freezing displayed after the cue was presented in the cued test was similar between the groups. Thus, the 5xFAD transgenic mice exhibited specific impairment in the hippocampus-dependent contextual fear conditioning test, and this phenotype wasimproved after TPPU treatment. Taken together

these results demonstrate that TPPU treatment rescued synaptic deficits, memory and cognitive behaviors in 5xFAD transgenic mice.

Discussion

Using postmortem human brain samples, primary cell cultures and two AD (5xFAD and APP^{NLGF} knock-in) mouse models, we investigated the role of sEH in neuroinflammation and AD pathogenesis and tested the therapeutic effect of an orally bioavailable small molecule sEH inhibitor, TPPU. We found that the amount of sEH was elevated in human AD postmortem brains and Aβ mouse models of AD. Increased sEH in 5xFAD transgenic mice correlated with lower amounts of EETs and EDPs. Pre-administration of EET or TPPU prevented acute LPS-induced neuroinflammation in these animals. Long-term TPPU treatment at the onset of AD neuropathology was able to reverse microglia and astrocyte activation and immune pathway dysregulation at the molecular, cellular and functional levels, and these changes were associated with attenuated Aβ pathology and improved synaptic and cognitive function. Moreover, TPPU treatment reinstated expression of and positively correlated with EpFA in the 5xFAD transgenic mouse brain, supporting the brain penetration and target engagement of TPPU.

Our results demonstrate that sEH was not only elevated in AD mouse models, but also was increased in human AD postmortem brains. Similar increases in sEH have also been reported in APP/PS1 AD mice in which genetic ablation of *Ephx2* was shown to ameliorate Aβ pathology and behavioral deficits (29). Whereas these aspects were consistent between our study and that of Lee et al. (29) (29), there were noticeable differences. Specifically, Lee et al. reported increased GFAP reactivity and altered APP/Aβ dynamics when *Ephx2* was deleted in APP/PS1 AD mice (29), whereas we detected reduced astrogliosis with no change in APP expression or processing upon TPPU treatment. Although the precise reason for the discrepancies is not clear, it is important to note that our approach involved pharmacological treatment of adult mice. In contrast, Lee et al. used genetic knockout mice in which *Ephx2* was deleted throughout life (29). Critically, sEH contains a C-terminal hydrolase and N-terminal phosphatase domain. *Ephx2* deletion ablated both activities, whereas TPPU and other sEH inhibitors only inactivated the hydrolase activity. In this regard, the Arg287Gln and Lys55Arg polymorphisms of sEH are associated with reduced phosphatase activity and increased risk for coronary heart disease and type 2 diabetes (48–51), suggesting a protective role of the sEH phosphatase domain. Thus, it is tempting to speculate that the increased astrogliosis and altered APP/Aβ pathway dynamics reported by Lee et al. may have been due to the loss of the sEH phosphatase activity.

Our cell-type specific analysis demonstrates that astrocytes are the predominant cells expressing sEH when it is deregulated in AD conditions. This leads to diminished EETs and EDPs and a reduction in their anti-inflammatory activities in both astrocytes and microglia. Besides the astrocytes, sEH is known to be highly expressed in the vasculature where it mediates vascular inflammation and barrier function through both EETs and EDPs (20, 52). Our expression analysis of sorted vascular endothelial cells revealed no appreciable differences in *Ephx2* expression between 5x FAD transgenic mice and nontransgenic controls, arguing against a major contribution of vascular sEH in disease pathogenesis.

Nevertheless, it remains possible that the overall therapeutic effect of TPPU was due to its inhibition of sEH in both astrocytes and vascular endothelium, and possibly other cell types as well. Interestingly, a recent report showed that liver sEH modulates depressive behaviors in mice, suggesting that sEH expressed in the peripheral system could influence brain function (53). As such, although our finding that TPPU entered the mouse brain and correlated with an increase in EETs and EDPs supported a CNS intrinsic mechanism, we cannot exclude the possibility that TPPU could also have exerted its effects through inhibition of liver sEH. The creation of mice with tissue-specific knockout of *Ephx2* in the astrocyte or liver is needed to address the cell-type specific effect (53).

Our Nanostring nCount panel analysis followed by qPCR validation revealed multiple immune and inflammatory response pathways were upregulated in the 5xFAD transgenic mice and downregulated by TPPU treatment. In addition, recent reports have identified a signaling pathway whereby microglia-mediated neuroinflammation, in a C1q-, IL-1α- and TNF-dependent manner, induced expression of A1 astrocyte genes that were toxic to the neurons (54–56). Our gene expression analysis revealed that a number of A1 astrocyte genes (*Serping1*, *Gbp2*, *Srgn*, *H2T23*, *Psmb8*) were normalized by TPPU treatment, suggesting that TPPU may reduce neuroinflammation by mitigating astrocyte activation, thus promoting neuronal survival. Additionally, NLRP3 inflammasome activation has been implicated in producing harmful chronic inflammatory reactions and impairing microglial Aβ clearance and cognitive function in AD (8, 57, 58). Indeed, we found that *Nlrp3* and *Casp1* were both upregulated in 5x FAD transgenic mouse brains and downregulated by TPPU treatment. Therefore, TPPU could suppress chronic neuroinflammation through NLRP3-dependent mechanisms.

We demonstrate here that long-term TPPU treatment not only dampened glia reactivity but also ameliorated Aβ pathology and improved functional outcomes in 5x FAD transgenic mice. Ample evidence documents that prolonged microglia activation leads to impaired Aβ phagocytosis and triggers the production of proinflammatory mediators, and that its inhibition reverses these anomalies (59, 60). Therefore, the observed reduction of Aβ pathology and improvement of neuronal function that we observed after TPPU treatment could be the consequences of glia normalization. Additionally, microglia, through complement-dependent mechanisms, have been shown to mediate synapse elimination (61, 62). Our gene expression analysis revealed that aberrant *C1q* and *C3* upregulation in 5xFAD transgenic mice was rescued by TPPU treatment (Fig. 4), and this correlated with increased Synaptophysin and PSD95positive synaptic puncta in the hippocampus (Fig. 7). Thus, the improved synaptic plasticity and behavioral performance in TPPU-treated 5xFAD transgenic mice could be attributed directly to TPPU by blocking complement-mediated synapse loss, which should be investigated in future experiments.

There are several limitations to our study. First, the precise mode of action, in particular whether TPPU's effect could be solely attributed to EET stabilization and how EETs mediate different biological functions, await further investigation. Second, we started the TPPU treatment at an early stage prior to the development of frank pathology. Whether TPPU remained effective when administrated at later times after amyloid pathology was already established was not addressed. Third, our results were obtained using 5xFAD

transgenic mice with numerous artificial features, including transgene overexpression and fast and aggressive Aβ pathology development. These caveats need to be taken into consideration when interpreting the results. Like all animal model studies, whether our findings can be recapitulated in humans requires further testing.

Several classes of sEH inhibitors have been developed (63). Overall, they are well-tolerated in preclinical studies, establishing a large safety window for targeting of sEH. Among these, TPPU is widely used as a tool compound because of its superior potency, specificity, and pharmacokinetics (31, 64–67). We report here that long-term administration of TPPU resulted in retention in the mouse brain where it engaged its sEH target and afforded beneficial effects in a mouse model of AD. These features make TPPU an attractive candidate for further development as a potential treatment for AD.

Materials and Methods

Study design

The goal of this study was to establish evidence in transgenic mouse models of AD that inhibition of the soluble epoxide hydrolase (sEH) with the small molecule inhibitor TPPU could modify amyloid pathology in mouse brains. The C57BL/6, and 5xFAD mice were obtained from the Jackson Laboratory (Bar Harbor, ME). APP^{NLGF} mice were obtained from RIKEN (33). Mice were housed 4–5 per cage in a pathogen free mouse facility with ad libitum access to food and water on a 12 hr light/dark cycle. Male and female mice at approximately equal ratio were used for all experiments except for Nanostring nCount panel experiments. Only males were used to achieve within group consistency for better cross group comparison..

The C57BL/6 mice were used to investigate the acute anti-inflammatory effects of both TPPU and EC-5026. To determine the chronic long term effects of TPPU on mitigating neuroinflammation, amyloid plaque pathology, synaptic abnormalities and behavioral deficits, 5xFAD transgenic mice were used. The APP^{NLGF} knock-in mice were used only to determine the changes in sEH protein expression. For mouse experiments, one individual would randomize the animals, plates, and slides, and another would analyze them. The minimum sample size for all experiments was held at six mice per group based on the design of previous studies (11). To improve our power, and thus our ability to statistically detect smaller effects, many of our analyses included more mice per group. In particular, 12 to 16 mice per experimental group were used for behavioral tests and six to nine mice per experimental group were randomly selected for biochemical analysis. All procedures were performed in accordance with NIH guidelines and approval of the Baylor College of Medicine Institutional Animal Care and Use Committee (IACUC). All in vitro experiments were performed at least twice, each with at least three technical repeats.

Postmortem brain tissues from AD patients and non-demented controls were provided by the University of Pennsylvania Center for Neurodegenerative Disease Research (CNDR). Informed consent was obtained from all subjects for the use of their postmortem tissues. The human AD and control demographic data can be found in Table S2. Influence of gender identity on the study results was not analyzed due to small sample size.

TPPU and EC5026 treatment

The sEH inhibitors TPPU was synthesized as described previously (31) and EC5026 was synthesized as described (International patent publication no. WO 2015/148954 A1). TPPU or EC5026 was dissolved either in DMSO for in vitro and ex vivo treatment (TPPU only) or in 1% polyethylene glycol 400 (PEG400, Fisher) for in vivo treatment. The vehicle mice received oral gavage treatment of 1% PEG400. Mice were perfused with saline before collecting brain for biochemical analysis. In the acute TPPU or EC5026 treatment regimen, ten- to twelve-week-old C57BL/6 mice received 1st dose of TPPU (3 mg/kg) via oral gavage 24 h before co-treatment of LPS (3 mg/kg, i.p.) and TPPU or EC5026 (2nd dose). Eighteen-hour post co-treatment, mice were sacrificed for analysis.

For long-term TPPU treatment, 5xFAD transgenic mice received TPPU (3mg/kg) in drinking water for either 2.5 months or 4.5 months starting at 2 months of age. The vehicle mice received 1% PEG400 in drinking water. Every two weeks, mice were supplied with a new water bottle containing fresh TPPU or vehicle solution.

Microglia and astrocyte monocultures and mixed culture

Primary glia cultures were prepared as described previously (61). In brief, mouse cortices and hippocampi were isolated from newborn pups (P0-P1) in dissection medium (HBSS with 10 mM HEPES, 1% v/v Pen/Strep) and cut into small pieces. Tissue was digested with 2.5% trypsin at 37°C for 15 min before trypsin inhibitor (1 mg/ml) was added. Next, tissue was centrifuged for 5 min at 1500 rpm, triturated, and resuspended in DMEM medium with 10% FBS. Cells were plated onto poly-D-lysine (PDL)-coated T-75 flasks at 50,000 cells/cm^2 to generate mixed glial cultures. For astrocyte and microglia co-culture, cells were trypsinized and seeded at 40,000 cells/cm^2 and cultured for 3–4 days in PDL-coated plates for mRNA assays or immunocytochemistry (ICC). For separation of microglia, confluent flasks were tapped on the table and floated cells which were mostly microglia were collected from the media. Microglia cells were then seeded at 50,000 cells/cm^2 and cultured for another day in PDL-coated 12-well plates for mRNA assays or on coverslips for staining. After collecting microglia cells, remaining cells (mostly astrocytes) were trypsinized and seeded at 40,000 cells/cm^2 and cultured for another two days in PDL-coated plated for mRNA assays or ICC.

RNA extraction and expression analysis

Total RNA was extracted from cells or human or mouse brain tissues using RNeasy Mini kit (Qiagen, 74106). Reverse transcription was carried out using iScript Reverse Transcription Supermix (Bio-Rad, 1708840). The qPCR analyses were performed using SYBR Green PCR master mix (Bio-Rad) on a CFX384 Touch Real-Time PCR Detection System. Primer sequences can be found in Supplementary Table 3.

For Nanostring nCounter panel analysis, RNA was isolated from 4.5-month-old male mouse hippocampus and 770 transcripts were quantified with the Nanostring nCounter multiplexed target platform using the Mouse Neuroinflammation panel (https://www.nanostring.com). nCounts of mRNA transcripts were normalized using the geometric means of 10 housekeeping genes (*Csnk2a2*, *Ccdc127*, *Xpnpep1*, *Lars*, *Supt7l*, *Tada2b*, *Aars*, *Mto1*, *Tbp*,

and *Fam104a*) and analyzed using nSolver 4.0 and the Advanced Analysis 2.0 plugin. Fold-change expression and p-values were calculated by linear regression analysis using negative binomial or log-linear models. P-values were corrected for multiple comparisons using the Benjamini-Yekutieli method. Volcano plots of differential expression data were plotted using the −log10 (p-value) and log2 fold-change using the Graphpad prism. Gene ontology enrichment analysis was performed using https://www.innatedb.com/. Heatmaps were constructed using Graphpad prism.

Griess assay for nitrite measurement

Griess assay was performed, as described previously (68). Briefly, standards in triplicate were used for each plate. Standard mix was made up of 1 ml media and 1 μl sodium nitrite and added to wells in volumes increasing by 5 μl from 0–35 μl. Media was added to each well to bring volume up to a total of 100 μl. Sample supernatant was added in duplicate to remaining wells in 100 μl. Then, 100 μl of Griess reagent (Sigma) was added to each well and incubated at RT for 20 minutes. Absorbance at 540 nm was detected in a Synergy 2 Multi-Detection Microplate Reader.

Cell-type purification and FACS sorting

Mice were perfused with ice-cold PBS, adult mouse brains (whole brain minus cerebellum) were chopped and resuspended in 2.5 ml of HBSS w/o Ca^{2+}, and w/o Mg^{2+} containing activated papain and DNase. Cell type purification and FACS sorting were done as described (34). Briefly, brains were incubated at 37°C, then triturated 4 times with a fire-polished glass Pasteur pipet. Next, samples were mixed with HBSS+ (HBSS + 0.5% BSA, 2mM EDTA) and centrifuged for 5 min. The pellet was resuspended in 1000 ml of HBSS+ and centrifuged for 15 sec at room temperature. The supernatant was collected and was filtered through cell strainer (BD SKU 352340) and centrifuged for 5 min at 300 g at 4°C. To remove myelin, the Miltenyi myelin removal beads were used according to the manufacturer's instructions (Miltenyi, 130-096-733). After that, cells were centrifuged at 300xG for 5 min at 4°C. Next, the cells were resuspended in 1ml HBSS+ solution and passed through a LS column. The total effluent was then centrifuged for 5 min at 300 g at 4°C to pellet the cells. For the antibody staining, the cells were resuspended in HBSS+ solution and then stained for with CD45-BV421 (BD, 563890), CD11b-FITC (BD, 553310) for microglia, ACSA-2-APC (Miltenyi, 130-102-315) for astrocytes, and cell viability blue fluorescent dye (Invitrogen, L23105). After FACS sorting, the cells were collected in Eppendorf tubes, centrifuged at 1500 rpm for 5 min, and resuspended in RLT buffer containing 1% BME for future qPCR analysis. The mRNA was extracted using the QIAGEN RNAEasy Micro kit (QIAGEN, 74004).

Immunofluorescence staining

Cells were fixed with 4% paraformaldehyde in 1X PBS for 15 min and processed for immunocytochemistry, as described previously (69). First, nonspecific sites were blocked with 0.2% bovine serum albumin, 0.5% Triton X-100, and 0.05% Tween 20 in PBS for 1 h at room temperature. Cells were then incubated with different primary antibodies: sEH (1:1000, Dr. Bruce Hammock lab (26)), GFAP (1:1000, Millipore), iNOS (1:500, Thermo Fisher), Iba-1 (1:1000, Wako) and COX-2 (1:1000, Thermo Fisher) at 4°C overnight.

Appropriate secondary antibodies (Alexa Fluor 488 or 555 or 647, Invitrogen) were used followed by incubation with DAPI to stain the nucleus. The coverslip-containing stained cells were washed twice with PBS and mounted on slides. After immunofluorescent staining, five individual areas from each coverslip were imaged using 20x magnification under a Leica TCS confocal microscope.

For mouse brain analysis, immunohistochemistry was performed on free-floating microtome-cut sections (30 μm in thickness), as described previously (68). Briefly, mice brains were post fixed in 4% paraformaldehyde overnight at 4°C and transferred to 30% sucrose solution following perfusion with saline. Sections were incubated with different antibodies: sEH (1:1000) (26), GFAP (1:1000, Millipore), iNOS (1:250, Thermo Fisher), Iba-1 (1:800, Wako or 1:500, Novus Biologicals), COX-2 (1:500, Thermo Fisher), CD68 (1:500, BioLegend), 6E10 (1:1000, BioLegend), Synaptophysin (1:500, Abcam), PSD95 (1:200, Millipore), NeuN (1:1000, Millipore), and Clec7a (1:50, Invivogen). Appropriate secondary antibodies (Alexa Fluor 488 or 594 or 647, Invitrogen) were used followed by incubation with DAPI. A total of three to four sections per brain containing the hippocampus and cortex and five to seven mice per group were stained with antibodies as mentioned above.

Image quantification

After immunofluorescence staining, confocal images were captured and mean intensity of fluorescence, number of immunoreactive cells and size of plaques were quantified using the Image J software (NIH). For quantification of 6E10 in the mouse cortex and hippocampus, sections were scanned using an EVOS FL Auto system. Images were then analyzed by ImageJ and background was subtracted by the software for fluorescence images before quantification. For synaptic marker co-localization studies, imaging was performed with a Leica confocal microscope, using a 63X oil objective with a 4.0 digital zoom in the CA3 region. Z-stacks of 5 μm thickness from the middle of the tissues (to avoid staining artifacts) were obtained with a 0.2 μm step-size, and 2 frame-averaged 512×512 images for each channel. Due to great variation in synaptic puncta densities by brain region, care was taken to image from the same areas consistently across all samples and experiments. Z-stacks with dual synaptic puncta labelling were analyzed using the ImageJ software. For NeuN+ve cells quantification, 8 images from each mouse (n=6 mice in each group) were counted manually. For Aβ plaque associated Iba+ve, CD68+ve, GFAP+ve, Clec7a+ve cells quantification, above mentioned marker+ve cells were counted within 100 μm radius of the 6E10+ve plaques. Total 86–123 plaques were counted in each group. Cell numbers were normalized to the plaques. All the images were captured and analyzed blindly using coded slides.

Western blotting

Cells or brain tissues were collected and resuspended in modified radioimmunoprecipitation (RIPA) assay buffer containing protease and phosphatase inhibitor mixture. Cell suspensions were sonicated after resuspension, whereas mouse brain tissues were homogenized, sonicated, and then centrifuged at 14,000 × g for 45 min at 4°C, as described previously (70). Briefly, protein concentrations were estimated using a BCA kit (Thermo Fisher). Lysates were separated on 7.5%–15% SDS-polyacrylamide electrophoresis gels (Bio-Rad).

After the separation, proteins were transferred to a nitrocellulose membrane, and nonspecific binding sites were blocked by treating with either Odyssey blocking buffer (LI-COR) or TBS with 5% bovine serum albumin (BSA) followed by antibody incubation: sEH (1:300, Santa Cruz or 1:1000, Hammock lab (26)), iNOS (1:1000, Cell signaling), GFAP (1:15000, EMD Millipore), Iba-1 (1:1200, Wako), Cox-2 (1:500, Thermo Fisher), 6E10 (for human APP, 1:1000, BioLegend), APP (recognizes APP-FL and CTF, 1:1000, Cell Signaling), Nicastrin (1:1000, Cell Signaling), PEN2 (1:1000, Cell Signaling), BACE1 (Cell Signaling), PS1 (1:1000, Cell Signaling), PS2 (1:1000, Cell Signaling) and β-actin (1:10,000, Sigma). Secondary IR-680-conjugated goat anti-mouse or goat anti-rabbit (1:10,000; Molecular Probes), IRDye 800-conjugated donkey anti-rabbit or donkey anti goat (1:10,000, Rockland, PA, USA) were used. Western blot images were captured with a LI-COR Odyssey machine (LI-COR). The western blot bands were quantified using ImageJ software (NIH).

Behavioral analysis

The novel object recognition protocol included three phases; habituation phase, a training phase and an object recognition phase. The habitation phase included of one session, 5 minutes in length, in which the animals were allowed to freely explore a small Plexiglas arena (measuring 22cm × 44cm) that was utilized in the training and testing phase. One day after habituation the animals underwent training. During the training phase, the animals were placed in the same arena with the addition of two identical objects. The animals were allowed to freely explore the objects for 5 minutes. 24 hours after the training phase, the test phase was initiated. During the testing phase, the animal was placed in the same arena with one object previously explored in the training phase, the familiar object, and one novel object differing in color and shape, but sharing a common size and volume. The animals were allowed to freely explore the objects for 5 minutes. ANY-Maze software was used to measure time spent exploring each object. Exploration of an object was defined by head orientation directed toward the object or physical contact with the object. The object discrimination ratio (ODR) was calculated by the following formula: ODR= (Time exploring specified object)/(time exploring novel object+ time exploring familiar object) × 100. The fear conditioning protocol involved a training phase, context test, and a cued test as previously described (71). During the training phase the mice were placed in the training chamber and allowed to freely explore the environment. At 3 minutes, an 80-dB white noise was presented as auditory conditioned stimulus for 30 seconds. During the last 2 seconds of the auditory stimulus, the unconditioned stimulus (US), a foot shock (0.8 mA, 2 seconds), was administered. The conditioned stimulus and unconditioned stimulus were then presented a second time at the 5-minute mark of the training procedure. After the second presentation of the unconditioned stimulus, the mice stayed in the training chamber for an additional 2 minutes without additional stimulations. The animals were returned to their original housing cages. 24 hours after the training procedure, the context test was performed. The mice were returned to the same training chamber consisting of the same context as the first procedure (same geometric shape of chamber, lights, scents and auditory sounds) for 3 minutes with no presentations of unconditioned stimulus or conditioned stimulus. One hour later, the cue test is performed. The cue test chamber consisted of a different geometric shape, flooring, light brightness and scent compared to the previous chamber used for training. After 3 minutes in the chamber, the auditory stimulus was presented for 3 minutes. The software,

FreezeFrame3 and FreezeView (San Diego Instruments) was used to record and analyze the percent freezing in each trial.

Electrophysiology

Field recordings of Schaffer collateral LTP was performed as described before (72). Briefly, brains were isolated from 6.5–7-month-old mice and cut into 400 mM slices on a vibratome. Hippocampal slices were incubated for 1 h at room temperature and then transferred to a heated recording chamber filled with recording ACSF (125 mM NaCl, 2.5 mM KCl, 1.25 mM NaH_2PO_4, 25 mM $NaHCO_3$, 1 mM $MgCl_2$, 2 mM $CaCl_2$, and 10 mM glucose, saturated with 95% O_2 and 5% CO_2) maintained at 32°C. Stimulation of Schaffer collaterals from the CA3 region was performed with bipolar electrodes, while borosilicate glass capillary pipettes filled with recording ACSF (resistances of 2–3.5 MΩ) were used to record field excitatory postsynaptic potentials (fEPSPs) in the CA1 region. Signals were amplified using a MultiClamp 700 B amplifier (Axon), digitized using a Digidata 1440A (Axon) with a 2 kHz low pass filter and a 3 Hz high pass filter and then captured and stored using Clampex 10.4 software (Axon) for offline data analysis. The genotypes and treatment groups were blinded to the experimenter. For each experiment 10–13 sections from 5–6 animals per group/genotype were used.

TPPU measurement and lipodomics

5xFAD mice were treated with TPPU (3 mg/kg) in drinking water for 4 months and then euthanized. Plasma and whole-brain homogenates were extracted and subjected to LC-MS/MS analysis of TPPU and oxylipin on a 4000 Qtrap LC-MS/MS instrument (Applied Biosystems Instrument Corporation). For drug analysis in plasma, 10 μl of plasma samples were transferred to 1.5 μl Eppendorf tubes containing 90 μl EDTA solution (0.1% EDTA and 0.1% acetic acid), spiked with 10μl of 1μg/ml TPPU-d3 in methanol, and subsequently subjected to liquid-liquid extraction by ethyl acetate (200 μl) twice (67). TPPU-d3 was added in each sample as an internal standard solution. The collected extraction solutions were dried using a speed vacuum concentrator, reconstituted in 50 μl of 100 nM CUDA in methanol, and ready for LC-MS/MS analysis. TPPU and oxylipin in brain tissues were analyzed simultaneously by a modified LC-MS/MS method(73) to including MRM transition of TPPU. Tissues (~50 mg) were homogenized in ice cold methanol with 0.1% BHT and 0.1% acetic acid. The homogenates were spiked with 10μl of internal standard solution (mixture of deuterated compounds) and stored at −80°C for 20hr. After that, the homogenates were extracted using solid-phase extraction (Oasis-HLB Cartridge, Waters). The extracted samples were then collected, dried and reconstituted in 50μl of 200 nM CUDA in methanol. The analytes were then detected by the modified LC-MS/MS method.

P-glycoprotein substrate evaluation

Caco-2 cells were diluted to 6.86×10^5 cells/mL with culture medium and 50 μl of cell suspension were dispensed into the filter well of the 96-well HTS Transwell plate. Cells were cultivated for 14–18 days in a cell culture incubator at 37°C, 5% CO_2, 95% relative humidity. Electrical resistance was measured across the monolayer by using Millicell Epithelial Volt-Ohm measuring system. “TEER of each well is calculated by the equation-TEER value (ohm•cm^2) = TEER measurement (ohms) × Area of membrane (cm^2). The

TEER value of each well should be greater than 230 ohms•cm^2. Digoxin was used as the reference substrate of P-gp. Propranolol was used as the high permeability marker. To determine the rate of drug transport in the apical to basolateral direction, working solutions containing TPPU was added to the Transwell insert (apical compartment). To determine the rate of drug transport in the basolateral to apical direction, working solutions containing TPPU was added to each well of the receiver plate. To determine the rate of drug transport in the presence of the P-gp inhibitor, verapamil the known inhibitor of Pgp, was added to both apical and basolateral compartments at a final concentration of 100 μM, followed by incubation at 37 °C for 2 hours. Next, samples from apical and basolateral wells were transferred to a new 96-well plate and cold acetonitrile containing appropriate internal standards (IS) were added into each well of the plate(s). Samples were analyzed by an LC-MS/MS. Percent parent compounds remaining at each time point are estimated by determining the peak area ratios from extracted ion chromatograms. The apparent permeability coefficient (P_{app}), in units of centimeter per second, using the following equation: P_{app} = (VA×[drug]acceptor)/(Area×Time×[drug]initial, donor), where VA is the volume (in ml) in the acceptor well, area is the surface area of the membrane (0.143 cm^2 for Transwell-96 Well Permeable Supports), and time is the total transport time in seconds. The efflux ratio was determined using the following equation: Efflux Ratio=P_{app}(B-A)/P_{app}(A-B), where P_{app} (B-A) indicates the apparent permeability coefficient in basolateral (B) to apical (A) direction, and P_{app} (A-B) indicates the apparent permeability coefficient in apical to basolateral direction. The recovery can be determined using the following equation: Recovery%=(VA×[drug]acceptor+VD×[drug]donor)/(VD×[drug]initial, donor), where VA is the volume (in ml) in the acceptor well (0.235 ml for Ap→Bl flux, and 0.075 ml for Bl→Ap), VD is the volume (in ml) in the donor well (0.075 ml for Ap→Bl flux, and 0.235 ml for Bl→Ap).

Quantification and statistical analysis

All data were analyzed with GraphPad Prism v.7.04 and presented as mean ± SEM (*P < 0.05, **P < 0.01, ***P < 0.001 and ****P < 0.0001). For simple comparisons, Student's t test was used. For multiple comparisons, ANOVA followed by the appropriate post hoc testing was utilized and is specified for each experiment in the figure legends. The statistical tests used for human gene expression analysis are specified in the human gene expression analysis methods section. All samples or animals were included in the statistical analysis unless otherwise specified.

Supplementary Material

Refer to Web version on PubMed Central for supplementary material.

Acknowledgements:

We are grateful to V. Lee and J. Trojanowski (University of Pennsylvania) for providing postmortem AD patient brain tissues and T. Saito and T. Saido (RIKEN Brain Science Institute) for the APP^{NLGF} knock-in mice. We thank B. Contreras and N. Aithmitti for expert technical assistance, B. Wang and E. Roy for help with organotypic culture and Nanostring nCount panel experiments, and members of the Zheng laboratory for insightful discussions. We acknowledge support from the Genomic and RNA Profiling Core and the Cytometry and Cell Sorting Core at Baylor College of Medicine for Nanostring and FACS analyses, respectively.

Funding: This project was supported by grants from the NIH (R01 NS093652, R01 AG020670, RF1 AG054111, R01 AG057509 and RF1 062257 to HZ) and NIEHS (RIVER Award R35 ES030443-01 and Superfund Research Program P42 ES04699 to BDH)

References

1. Querfurth HW, LaFerla FM, Alzheimer's disease. N Engl J Med 362, 329–344 (2010). [PubMed: 20107219]
2. Long JM, Holtzman DM, Alzheimer Disease: An Update on Pathobiology and Treatment Strategies. Cell 179, 312–339 (2019). [PubMed: 31564456]
3. Mucke L, Selkoe DJ, Neurotoxicity of amyloid beta-protein: synaptic and network dysfunction. Cold Spring Harb Perspect Med 2, a006338 (2012). [PubMed: 22762015]
4. Cummings JL, Cohen S, van Dyck CH, Brody M, Curtis C, Cho W, Ward M, Friesenhahn M, Rabe C, Brunstein F, Quartino A, Honigberg LA, Fuji RN, Clayton D, Mortensen D, Ho C, Paul R, ABBY: A phase 2 randomized trial of crenezumab in mild to moderate Alzheimer disease. Neurology 90, e1889–e1897 (2018). [PubMed: 29695589]
5. Cummings JL, Morstorf T, Zhong K, Alzheimer's disease drug-development pipeline: few candidates, frequent failures. Alzheimers Res Ther 6, 37 (2014). [PubMed: 25024750]
6. Elmaleh DR, Farlow MR, Conti PS, Tompkins RG, Kundakovic L, Tanzi RE, Developing Effective Alzheimer's Disease Therapies: Clinical Experience and Future Directions. J Alzheimers Dis 71, 715–732 (2019). [PubMed: 31476157]
7. Guillot-Sestier MV, Doty KR, Town T, Innate Immunity Fights Alzheimer's Disease. Trends Neurosci 38, 674–681 (2015). [PubMed: 26549882]
8. Heneka MT, Kummer MP, Stutz A, Delekate A, Schwartz S, Vieira-Saecker A, Griep A, Axt D, Remus A, Tzeng TC, Gelpi E, Halle A, Korte M, Latz E, Golenbock DT, NLRP3 is activated in Alzheimer's disease and contributes to pathology in APP/PS1 mice. Nature 493, 674–678 (2013). [PubMed: 23254930]
9. Heneka MT, Kummer MP, Latz E, Innate immune activation in neurodegenerative disease. Nat Rev Immunol 14, 463–477 (2014). [PubMed: 24962261]
10. Prokop S, Miller KR, Heppner FL, Microglia actions in Alzheimer's disease. Acta Neuropathol 126, 461–477 (2013). [PubMed: 24224195]
11. Lian H, Zheng H, Signaling pathways regulating neuron-glia interaction and their implications in Alzheimer's disease. J Neurochem 136, 475–491 (2016). [PubMed: 26546579]
12. Kunkle BW, Grenier-Boley B, Sims R, Bis JC, Damotte V, Naj AC, Boland A, Vronskaya M, van der Lee SJ, Amlie-Wolf A, Bellenguez C, Frizatti A, Chouraki V, Martin ER, Sleegers K, Badarinarayan N, Jakobsdottir J, Hamilton-Nelson KL, Moreno-Grau S, Olaso R, Raybould R, Chen Y, Kuzma AB, Hiltunen M, Morgan T, Ahmad S, Vardarajan BN, Epelbaum J, Hoffmann P, Boada M, Beecham GW, Garnier JG, Harold D, Fitzpatrick AL, Valladares O, Moutet ML, Gerrish A, Smith AV, Qu L, Bacq D, Denning N, Jian X, Zhao Y, Del Zompo M, Fox NC, Choi SH, Mateo I, Hughes JT, Adams HH, Malamon J, Sanchez-Garcia F, Patel Y, Brody JA, Dombroski BA, Naranjo MCD, Daniilidou M, Eiriksdottir G, Mukherjee S, Wallon D, Uphill J, Aspelund T, Cantwell LB, Garzia F, Galimberti D, Hofer E, Butkiewicz M, Fin B, Scarpini E, Sarnowski C, Bush WS, Meslage S, Kornhuber J, White CC, Song Y, Barber RC, Engelborghs S, Sordon S, Voijnovic D, Adams PM, Vandenberghe R, Mayhaus M, Cupples LA, Albert MS, De Deyn PP, Gu W, Himali JJ, Beekly D, Squassina A, Hartmann AM, Orellana A, Blacker D, Rodriguez-Rodriguez E, Lovestone S, Garcia ME, Doody RS, Munoz-Fernadez C, Sussams R, Lin H, Fairchild TJ, Benito YA, Holmes C, Karamujic-Comic H, Frosch MP, Thonberg H, Maier W, Roshchupkin G, Ghetti B, Giedraitis V, Kawalia A, Li S, Huebinger RM, Kilander L, Moebus S, Hernandez I, Kamboh MI, Brundin R, Turton J, Yang Q, Katz MJ, Concari L, Lord J, Beiser AS, Keene CD, Helisalmi S, Kloszewska I, Kukull WA, Koivisto AM, Lynch A, Tarraga L, Larson EB, Haapasalo A, Lawlor B, Mosley TH, Lipton RB, Solfrizzi V, Gill M, Longstreth WT Jr., Montine TJ, Frisardi V, Diez-Fairen M, Rivadeneira F, Petersen RC, Deramecourt V, Alvarez I, Salani F, Ciaramella A, Boerwinkle E, Reiman EM, Fievet N, Rotter JI, Reisch JS, Hanon O, Cupidi C, Andre Uitterlinden AG, Royall DR, Dufouil C, Maletta RG, de Rojas I, Sano M, Brice A, Cecchetti R, George-Hyslop PS, Ritchie K, Tsolaki M, Tsuang DW, Dubois B, Craig D, Wu CK,

Soininen H, Avramidou D, Albin RL, Fratiglioni L, Germanou A, Apostolova LG, Keller L, Koutroumani M, Arnold SE, Panza F, Gkatzima O, Asthana S, Hannequin D, Whitehead P, Atwood CS, Caffarra P, Hampel H, Quintela I, Carracedo A, Lannfelt L, Rubinsztein DC, Barnes LL, Pasquier F, Frolich L, Barral S, McGuinness B, Beach TG, Johnston JA, Becker JT, Passmore P, Bigio EH, Schott JM, Bird TD, Warren JD, Boeve BF, Lupton MK, Bowen JD, Proitsi P, Boxer A, Powell JF, Burke JR, Kauwe JSK, Burns JM, Mancuso M, Buxbaum JD, Bonuccelli U, Cairns NJ, McQuillin A, Cao C, Livingston G, Carlson CS, Bass NJ, Carlsson CM, Hardy J, Carney RM, Bras J, Carrasquillo MM, Guerreiro R, Allen M, Chui HC, Fisher E, Masullo C, Crocco EA, DeCarli C, Bisceglio G, Dick M, Ma L, Duara R, Graff-Radford NR, Evans DA, Hodges A, Faber KM, Scherer M, Fallon KB, Riemenschneider M, Fardo DW, Heun R, Farlow MR, Kolsch H, Ferris S, Leber M, Foroud TM, Heuser I, Galasko DR, Giegling I, Gearing M, Hull M, Geschwind DH, Gilbert JR, Morris J, Green RC, Mayo K, Growdon JH, Feulner T, Hamilton RL, Harrell LE, Drichel D, Honig LS, Cushion TD, Huentelman MJ, Hollingworth P, Hulette CM, Hyman BT, Marshall R, Jarvik GP, Meggy A, Abner E, Menzies GE, Jin LW, Leonenko G, Real LM, Jun GR, Baldwin CT, Grozeva D, Karydas A, Russo G, Kaye JA, Kim R, Jessen F, Kowall NW, Vellas B, Kramer JH, Vardy E, LaFerla FM, Jockel KH, Lah JJ, Dichgans M, Leverenz JB, Mann D, Levey AI, Pickering-Brown S, Lieberman AP, Klopp N, Lunetta KL, Wichmann HE, Lyketsos CG, Morgan K, Marson DC, Brown K, Martiniuk F, Medway C, Mash DC, Nothen MM, Masliah E, Hooper NM, McCormick WC, Daniele A, McCurry SM, Bayer A, McDavid AN, Gallacher J, McKee AC, van den Bussche H, Mesulam M, Brayne C, Miller BL, Riedel-Heller S, Miller CA, Miller JW, Al-Chalabi A, Morris JC, Shaw CE, Myers AJ, Wiltfang J, O'Bryant S, Olichney JM, Alvarez V, Parisi JE, Singleton AB, Paulson HL, Collinge J, Perry WR, Mead S, Peskind E, Cribbs DH, Rossor M, Pierce A, Ryan NS, Poon WW, Nacmias B, Potter H, Sorbi S, Quinn JF, Sacchinelli E, Raj A, Spalletta G, Raskind M, Caltagirone C, Bossu P, Orfei MD, Reisberg B, Clarke R, Reitz C, Smith AD, Ringman JM, Warden D, Roberson ED, Wilcock G, Rogaeva E, Bruni AC, Rosen HJ, Gallo M, Rosenberg RN, Ben-Shlomo Y, Sager MA, Mecocci P, Saykin AJ, Pastor P, Cuccaro ML, Vance JM, Schneider JA, Schneider LS, Slifer S, Seeley WW, Smith AG, Sonnen JA, Spina S, Stern RA, Swerdlow RH, Tang M, Tanzi RE, Trojanowski JQ, Troncoso JC, Van Deerlin VM, Van Eldik LJ, Vinters HV, Vonsattel JP, Weintraub S, Welsh-Bohmer KA, Wilhelmsen KC, Williamson J, Wingo TS, Woltjer RL, Wright CB, Yu CE, Yu L, Saba Y, Pilotto A, Bullido MJ, Peters O, Crane PK, Bennett D, Bosco P, Coto E, Boccardi V, De Jager PL, Lleo A, Warner N, Lopez OL, Ingelsson M, Deloukas P, Cruchaga C, Graff C, Gwilliam R, Fornage M, Goate AM, Sanchez-Juan P, Kehoe PG, Amin N, Ertekin-Taner N, Berr C, Debette S, Love S, Launer LJ, Younkin SG, Dartigues JF, Corcoran C, Ikram MA, Dickson DW, Nicolas G, Campion D, Tschanz J, Schmidt H, Hakonarson H, Clarimon J, Munger R, Schmidt R, Farrer LA, Van Broeckhoven C, C. O. D. M, DeStefano AL, Jones L, Haines JL, Deleuze JF, Owen MJ, Gudnason V, Mayeux R, Escott-Price V, Psaty BM, Ramirez A, Wang LS, Ruiz A, van Duijn CM, Holmans PA, Seshadri S, Williams J, Amouyel P, Schellenberg GD, Lambert JC, Pericak-Vance MA, Genetic meta-analysis of diagnosed Alzheimer's disease identifies new risk loci and implicates Abeta, tau, immunity and lipid processing. Nat Genet 51, 414–430 (2019). [PubMed: 30820047]

13. Liu C, Chyr J, Zhao W, Xu Y, Ji Z, Tan H, Soto C, Zhou X, Genome-Wide Association and Mechanistic Studies Indicate That Immune Response Contributes to Alzheimer's Disease Development. Front Genet 9, 410 (2018). [PubMed: 30319691]
14. Guerreiro R, Bras J, Hardy J, SnapShot: genetics of Alzheimer's disease. Cell 155, 968–968.e961 (2013). [PubMed: 24209629]
15. Felsky D, Roostaei T, Nho K, Risacher SL, Bradshaw EM, Petyuk V, Schneider JA, Saykin A, Bennett DA, De Jager PL, Neuropathological correlates and genetic architecture of microglial activation in elderly human brain. Nat Commun 10, 409 (2019). [PubMed: 30679421]
16. Trepanier CH, Milgram NW, Neuroinflammation in Alzheimer's disease: are NSAIDs and selective COX-2 inhibitors the next line of therapy? J Alzheimers Dis 21, 1089–1099 (2010). [PubMed: 21504126]
17. Cacciatore I, Marinelli L, Fornasari E, Cerasa LS, Eusepi P, Turkez H, Pomilio C, Reale M, D'Angelo C, Costantini E, Di Stefano A, Novel NSAID-Derived Drugs for the Potential Treatment of Alzheimer's Disease. Int J Mol Sci 17, (2016).

18. Shen HC, Hammock BD, Discovery of inhibitors of soluble epoxide hydrolase: a target with multiple potential therapeutic indications. J Med Chem 55, 1789–1808 (2012). [PubMed: 22168898]
19. Phillis JW, Horrocks LA, Farooqui AA, Cyclooxygenases, lipoxygenases, and epoxygenases in CNS: their role and involvement in neurological disorders. Brain Res Rev 52, 201–243 (2006). [PubMed: 16647138]
20. Node K, Huo Y, Ruan X, Yang B, Spiecker M, Ley K, Zeldin DC, Liao JK, Anti-inflammatory properties of cytochrome P450 epoxygenase-derived eicosanoids. Science 285, 1276–1279 (1999). [PubMed: 10455056]
21. Bystrom J, Wray JA, Sugden MC, Holness MJ, Swales KE, Warner TD, Edin ML, Zeldin DC, Gilroy DW, Bishop-Bailey D, Endogenous epoxygenases are modulators of monocyte/macrophage activity. PLoS One 6, e26591 (2011). [PubMed: 22028915]
22. Schmelzer KR, Kubala L, Newman JW, Kim IH, Eiserich JP, Hammock BD, Soluble epoxide hydrolase is a therapeutic target for acute inflammation. Proc Natl Acad Sci U S A 102, 9772–9777 (2005). [PubMed: 15994227]
23. Fang X, Soluble epoxide hydrolase: a novel target for the treatment of hypertension. Recent Pat Cardiovasc Drug Discov 1, 67–72 (2006). [PubMed: 18221075]
24. Ng VY, Huang Y, Reddy LM, Falck JR, Lin ET, Kroetz DL, Cytochrome P450 eicosanoids are activators of peroxisome proliferator-activated receptor alpha. Drug Metab Dispos 35, 1126–1134 (2007). [PubMed: 17431031]
25. Harris TR, Hammock BD, Soluble epoxide hydrolase: gene structure, expression and deletion. Gene 526, 61–74 (2013). [PubMed: 23701967]
26. Ren Q, Ma M, Ishima T, Morisseau C, Yang J, Wagner KM, Zhang JC, Yang C, Yao W, Dong C, Han M, Hammock BD, Hashimoto K, Gene deficiency and pharmacological inhibition of soluble epoxide hydrolase confers resilience to repeated social defeat stress. Proc Natl Acad Sci U S A 113, E1944–1952 (2016). [PubMed: 26976569]
27. Ma M, Ren Q, Yang J, Zhang K, Xiong Z, Ishima T, Pu Y, Hwang SH, Toyoshima M, Iwayama Y, Hisano Y, Yoshikawa T, Hammock BD, Hashimoto K, Key role of soluble epoxide hydrolase in the neurodevelopmental disorders of offspring after maternal immune activation. Proc Natl Acad Sci U S A 116, 7083–7088 (2019). [PubMed: 30890645]
28. Ren Q, Ma M, Yang J, Nonaka R, Yamaguchi A, Ishikawa KI, Kobayashi K, Murayama S, Hwang SH, Saiki S, Akamatsu W, Hattori N, Hammock BD, Hashimoto K, Soluble epoxide hydrolase plays a key role in the pathogenesis of Parkinson's disease. Proc Natl Acad Sci U S A 115, E5815–e5823 (2018). [PubMed: 29735655]
29. Lee HT, Lee KI, Chen CH, Lee TS, Genetic deletion of soluble epoxide hydrolase delays the progression of Alzheimer's disease. J Neuroinflammation 16, 267 (2019). [PubMed: 31847859]
30. Griñán-Ferré C, Codony S, Pujol E, Yang J, Leiva R, Escolano C, Puigoriol-Illamola D, Companys-Alemany J, Corpas R, Sanfeliu C, Pérez B, Loza MI, Brea J, Morisseau C, Hammock BD, Vázquez S, Pallàs M, Galdeano C, Pharmacological Inhibition of Soluble Epoxide Hydrolase as a New Therapy for Alzheimer's Disease. Neurotherapeutics, (2020).
31. Rose TE, Morisseau C, Liu JY, Inceoglu B, Jones PD, Sanborn JR, Hammock BD, 1-Aryl-3-(1-acylpiperidin-4-yl)urea inhibitors of human and murine soluble epoxide hydrolase: structure-activity relationships, pharmacokinetics, and reduction of inflammatory pain. J Med Chem 53, 7067–7075 (2010). [PubMed: 20812725]
32. Rapoport SI, Arachidonic acid and the brain. J Nutr 138, 2515–2520 (2008). [PubMed: 19022981]
33. Saito T, Matsuba Y, Mihira N, Takano J, Nilsson P, Itohara S, Iwata N, Saido TC, Single App knock-in mouse models of Alzheimer's disease. Nat Neurosci 17, 661–663 (2014). [PubMed: 24728269]
34. Swartzlander DB, Propson NE, Roy ER, Saito T, Saido T, Wang B, Zheng H, Concurrent cell type-specific isolation and profiling of mouse brains in inflammation and Alzheimer's disease. JCI Insight 3, (2018).
35. Yang W, Tuniki VR, Anjaiah S, Falck JR, Hillard CJ, Campbell WB, Characterization of epoxyeicosatrienoic acid binding site in U937 membranes using a novel radiolabeled agonist, 20–

125i-14,15-epoxyeicosa-8(Z)-enoic acid. J Pharmacol Exp Ther 324, 1019–1027 (2008). [PubMed: 18171909]

36. Gauthier KM, Deeter C, Krishna UM, Reddy YK, Bondlela M, Falck JR, Campbell WB, 14,15-Epoxyeicosa-5(Z)-enoic acid: a selective epoxyeicosatrienoic acid antagonist that inhibits endothelium-dependent hyperpolarization and relaxation in coronary arteries. Circ Res 90, 1028–1036 (2002). [PubMed: 12016270]
37. Gauthier KM, Jagadeesh SG, Falck JR, Campbell WB, 14,15-epoxyeicosa-5(Z)-enoic-mSI: a 14,15- and 5,6-EET antagonist in bovine coronary arteries. Hypertension 42, 555–561 (2003). [PubMed: 12953017]
38. Hung TH, Shyue SK, Wu CH, Chen CC, Lin CC, Chang CF, Chen SF, Deletion or inhibition of soluble epoxide hydrolase protects against brain damage and reduces microglia-mediated neuroinflammation in traumatic brain injury. Oncotarget 8, 103236–103260 (2017). [PubMed: 29262558]
39. Rosenberg MF, Velarde G, Ford RC, Martin C, Berridge G, Kerr ID, Callaghan R, Schmidlin A, Wooding C, Linton KJ, Higgins CF, Repacking of the transmembrane domains of P-glycoprotein during the transport ATPase cycle. Embo j 20, 5615–5625 (2001). [PubMed: 11598005]
40. Balimane PV, Han YH, Chong S, Current industrial practices of assessing permeability and P-glycoprotein interaction. Aaps j 8, E1–13 (2006). [PubMed: 16584115]
41. Elsby R, Surry DD, Smith VN, Gray AJ, Validation and application of Caco-2 assays for the in vitro evaluation of development candidate drugs as substrates or inhibitors of P-glycoprotein to support regulatory submissions. Xenobiotica 38, 1140–1164 (2008). [PubMed: 18668443]
42. Williams L, Bradley L, Smith A, Foxwell B, Signal transducer and activator of transcription 3 is the dominant mediator of the anti-inflammatory effects of IL-10 in human macrophages. J Immunol 172, 567–576 (2004). [PubMed: 14688368]
43. Krasemann S, Madore C, Cialic R, Baufeld C, Calcagno N, El Fatimy R, Beckers L, O'Loughlin E, Xu Y, Fanek Z, Greco DJ, Smith ST, Tweet G, Humulock Z, Zrzavy T, Conde-Sanroman P, Gacias M, Weng Z, Chen H, Tjon E, Mazaheri F, Hartmann K, Madi A, Ulrich JD, Glatzel M, Worthmann A, Heeren J, Budnik B, Lemere C, Ikezu T, Heppner FL, Litvak V, Holtzman DM, Lassmann H, Weiner HL, Ochando J, Haass C, Butovsky O, The TREM2-APOE Pathway Drives the Transcriptional Phenotype of Dysfunctional Microglia in Neurodegenerative Diseases. Immunity 47, 566–581.e569 (2017). [PubMed: 28930663]
44. Oakley H, Cole SL, Logan S, Maus E, Shao P, Craft J, Guillozet-Bongaarts A, Ohno M, Disterhoft J, Van Eldik L, Berry R, Vassar R, Intraneuronal beta-amyloid aggregates, neurodegeneration, and neuron loss in transgenic mice with five familial Alzheimer's disease mutations: potential factors in amyloid plaque formation. J Neurosci 26, 10129–10140 (2006). [PubMed: 17021169]
45. Mariani MM, Malm T, Lamb R, Jay TR, Neilson L, Casali B, Medarametla L, Landreth GE, Neuronally-directed effects of RXR activation in a mouse model of Alzheimer's disease. Sci Rep 7, 42270 (2017). [PubMed: 28205585]
46. Kim S, Nam Y, Jeong YO, Park HH, Lee SK, Shin SJ, Jung H, Kim BH, Hong SB, Park YH, Kim J, Yu J, Yoo DH, Park SH, Jeon SG, Moon M, Topographical Visualization of the Reciprocal Projection between the Medial Septum and the Hippocampus in the 5XFAD Mouse Model of Alzheimer's Disease. Int J Mol Sci 20, (2019).
47. Eimer WA, Vassar R, Neuron loss in the 5XFAD mouse model of Alzheimer's disease correlates with intraneuronal Aβ42 accumulation and Caspase-3 activation. Mol Neurodegener 8, 2 (2013). [PubMed: 23316765]
48. Przybyla-Zawislak BD, Srivastava PK, Vazquez-Matias J, Mohrenweiser HW, Maxwell JE, Hammock BD, Bradbury JA, Enayetallah AE, Zeldin DC, Grant DF, Polymorphisms in human soluble epoxide hydrolase. Mol Pharmacol 64, 482–490 (2003). [PubMed: 12869654]
49. Srivastava PK, Sharma VK, Kalonia DS, Grant DF, Polymorphisms in human soluble epoxide hydrolase: effects on enzyme activity, enzyme stability, and quaternary structure. Arch Biochem Biophys 427, 164–169 (2004). [PubMed: 15196990]
50. Fornage M, Boerwinkle E, Doris PA, Jacobs D, Liu K, Wong ND, Polymorphism of the soluble epoxide hydrolase is associated with coronary artery calcification in African-American subjects: The Coronary Artery Risk Development in Young Adults (CARDIA) study. Circulation 109, 335–339 (2004). [PubMed: 14732757]

51. Ohtoshi K, Kaneto H, Node K, Nakamura Y, Shiraiwa T, Matsuhisa M, Yamasaki Y, Association of soluble epoxide hydrolase gene polymorphism with insulin resistance in type 2 diabetic patients. Biochem Biophys Res Commun 331, 347–350 (2005). [PubMed: 15845398]
52. Hu J, Dziumbla S, Lin J, Bibli SI, Zukunft S, de Mos J, Awwad K, Fromel T, Jungmann A, Devraj K, Cheng Z, Wang L, Fauser S, Eberhart CG, Sodhi A, Hammock BD, Liebner S, Muller OJ, Glaubitz C, Hammes HP, Popp R, Fleming I, Inhibition of soluble epoxide hydrolase prevents diabetic retinopathy. Nature 552, 248–252 (2017). [PubMed: 29211719]
53. Qin XH, Wu Z, Dong JH, Zeng YN, Xiong WC, Liu C, Wang MY, Zhu MZ, Chen WJ, Zhang Y, Huang QY, Zhu XH, Liver Soluble Epoxide Hydrolase Regulates Behavioral and Cellular Effects of Chronic Stress. Cell Rep 29, 3223–3234.e3226 (2019). [PubMed: 31801085]
54. Liddelow SA, Guttenplan KA, Clarke LE, Bennett FC, Bohlen CJ, Schirmer L, Bennett ML, Munch AE, Chung WS, Peterson TC, Wilton DK, Frouin A, Napier BA, Panicker N, Kumar M, Buckwalter MS, Rowitch DH, Dawson VL, Dawson TM, Stevens B, Barres BA, Neurotoxic reactive astrocytes are induced by activated microglia. Nature 541, 481–487 (2017). [PubMed: 28099414]
55. Clarke LE, Liddelow SA, Neurobiology: Diversity reaches the stars. Nature 548, 396–397 (2017). [PubMed: 28836597]
56. Shi Y, Yamada K, Liddelow SA, Smith ST, Zhao L, Luo W, Tsai RM, Spina S, Grinberg LT, Rojas JC, Gallardo G, Wang K, Roh J, Robinson G, Finn MB, Jiang H, Sullivan PM, Baufeld C, Wood MW, Sutphen C, McCue L, Xiong C, Del-Aguila JL, Morris JC, Cruchaga C, Fagan AM, Miller BL, Boxer AL, Seeley WW, Butovsky O, Barres BA, Paul SM, Holtzman DM, ApoE4 markedly exacerbates tau-mediated neurodegeneration in a mouse model of tauopathy. Nature 549, 523–527 (2017). [PubMed: 28959956]
57. Tejera D, Mercan D, Sanchez-Caro JM, Hanan M, Greenberg D, Soreq H, Latz E, Golenbock D, Heneka MT, Systemic inflammation impairs microglial Abeta clearance through NLRP3 inflammasome. Embo j 38, e101064 (2019). [PubMed: 31359456]
58. Park MH, Lee M, Nam G, Kim M, Kang J, Choi BJ, Jeong MS, Park KH, Han WH, Tak E, Kim MS, Lee J, Lin Y, Lee YH, Song IS, Choi MK, Lee JY, Jin HK, Bae JS, Lim MH, N,N'-Diacetyl-p-phenylenediamine restores microglial phagocytosis and improves cognitive defects in Alzheimer's disease transgenic mice. Proc Natl Acad Sci U S A 116, 23426–23436 (2019). [PubMed: 31685616]
59. Salter MW, Stevens B, Microglia emerge as central players in brain disease. Nat Med 23, 1018–1027 (2017). [PubMed: 28886007]
60. Sarlus H, Heneka MT, Microglia in Alzheimer's disease. J Clin Invest 127, 3240–3249 (2017). [PubMed: 28862638]
61. Litvinchuk A, Wan YW, Swartzlander DB, Chen F, Cole A, Propson NE, Wang Q, Zhang B, Liu Z, Zheng H, Complement C3aR Inactivation Attenuates Tau Pathology and Reverses an Immune Network Deregulated in Tauopathy Models and Alzheimer's Disease. Neuron 100, 1337–1353.e1335 (2018). [PubMed: 30415998]
62. Shi Q, Chowdhury S, Ma R, Le KX, Hong S, Caldarone BJ, Stevens B, Lemere CA, Complement C3 deficiency protects against neurodegeneration in aged plaque-rich APP/PS1 mice. Sci Transl Med 9, (2017).
63. Zarriello S, Tuazon JP, Corey S, Schimmel S, Rajani M, Gorsky A, Incontri D, Hammock BD, Borlongan CV, Humble beginnings with big goals: Small molecule soluble epoxide hydrolase inhibitors for treating CNS disorders. Prog Neurobiol 172, 23–39 (2019). [PubMed: 30447256]
64. Ulu A, Appt S, Morisseau C, Hwang SH, Jones PD, Rose TE, Dong H, Lango J, Yang J, Tsai HJ, Miyabe C, Fortenbach C, Adams MR, Hammock BD, Pharmacokinetics and in vivo potency of soluble epoxide hydrolase inhibitors in cynomolgus monkeys. Br J Pharmacol 165, 1401–1412 (2012). [PubMed: 21880036]
65. Liu Y, Lu X, Nguyen S, Olson JL, Webb HK, Kroetz DL, Epoxyeicosatrienoic acids prevent cisplatin-induced renal apoptosis through a p38 mitogen-activated protein kinase-regulated mitochondrial pathway. Mol Pharmacol 84, 925–934 (2013). [PubMed: 24092818]
66. Lee KS, Liu JY, Wagner KM, Pakhomova S, Dong H, Morisseau C, Fu SH, Yang J, Wang P, Ulu A, Mate CA, Nguyen LV, Hwang SH, Edin ML, Mara AA, Wulff H, Newcomer ME, Zeldin DC,

Hammock BD, Optimized inhibitors of soluble epoxide hydrolase improve in vitro target residence time and in vivo efficacy. J Med Chem 57, 7016–7030 (2014). [PubMed: 25079952]

67. Wan D, Yang J, McReynolds CB, Barnych B, Wagner KM, Morisseau C, Hwang SH, Sun J, Blocher R, Hammock BD, In vitro and in vivo Metabolism of a Potent Inhibitor of Soluble Epoxide Hydrolase, 1-(1-Propionylpiperidin-4-yl)-3-(4-(trifluoromethoxy)phenyl)urea. Front Pharmacol 10, 464 (2019). [PubMed: 31143115]
68. Ghosh A, Tyson T, George S, Hildebrandt EN, Steiner JA, Madaj Z, Schulz E, Machiela E, McDonald WG, Escobar Galvis ML, Kordower JH, Van Raamsdonk JM, Colca JR, Brundin P, Mitochondrial pyruvate carrier regulates autophagy, inflammation, and neurodegeneration in experimental models of Parkinson's disease. Sci Transl Med 8, 368ra174 (2016).
69. Ghosh A, Langley MR, Harischandra DS, Neal ML, Jin H, Anantharam V, Joseph J, Brenza T, Narasimhan B, Kanthasamy A, Kalyanaraman B, Kanthasamy AG, Mitoapocynin Treatment Protects Against Neuroinflammation and Dopaminergic Neurodegeneration in a Preclinical Animal Model of Parkinson's Disease. J Neuroimmune Pharmacol 11, 259–278 (2016). [PubMed: 26838361]
70. Ghosh A, Kanthasamy A, Joseph J, Anantharam V, Srivastava P, Dranka BP, Kalyanaraman B, Kanthasamy AG, Anti-inflammatory and neuroprotective effects of an orally active apocynin derivative in pre-clinical models of Parkinson's disease. J Neuroinflammation 9, 241 (2012). [PubMed: 23092448]
71. Guo W, Allan AM, Zong R, Zhang L, Johnson EB, Schaller EG, Murthy AC, Goggin SL, Eisch AJ, Oostra BA, Nelson DL, Jin P, Zhao X, Ablation of Fmrp in adult neural stem cells disrupts hippocampus-dependent learning. Nat Med 17, 559–565 (2011). [PubMed: 21516088]
72. Lian H, Yang L, Cole A, Sun L, Chiang AC, Fowler SW, Shim DJ, Rodriguez-Rivera J, Taglialatela G, Jankowsky JL, Lu HC, Zheng H, NFkappaB-activated astroglial release of complement C3 compromises neuronal morphology and function associated with Alzheimer's disease. Neuron 85, 101–115 (2015). [PubMed: 25533482]
73. Yang J, Schmelzer K, Georgi K, Hammock BD, Quantitative profiling method for oxylipin metabolome by liquid chromatography electrospray ionization tandem mass spectrometry. Anal Chem 81, 8085–8093 (2009). [PubMed: 19715299]

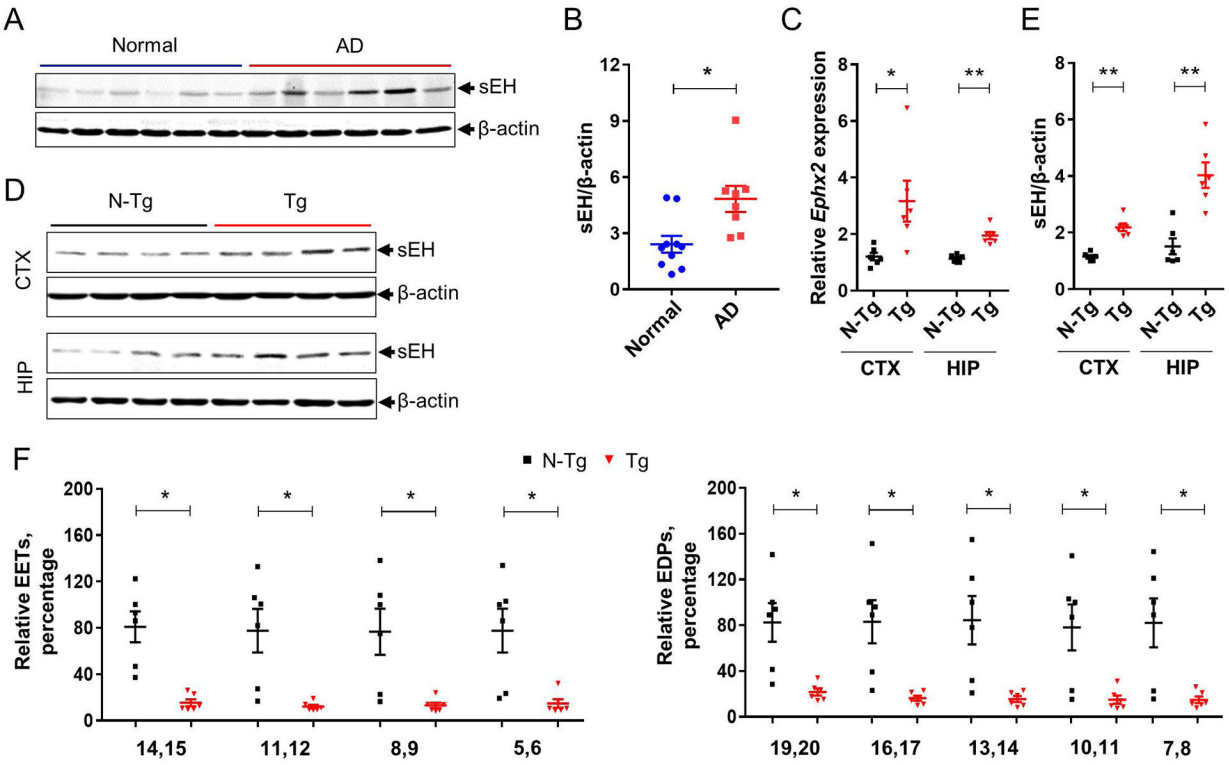

Fig. 1. Dysregulation of sEH and EETs in AD.

(A) Representative Western blot illustrating the expression of sEH in postmortem brain tissue from AD patients (n=6) and age-matched cognitively normal controls (n=6). β-actin was used as a loading control. (B) Quantification of the sEH/β-actin ratio in the Western blot from panel A C. (C) qPCR analysis of *Ephx2* expression in cortex (CTX) and in hippocampus (HIP) of littermate non-transgenic (N-Tg) and 5xFAD transgenic (Tg) mice at 4.5 months of age. (D) Representative Western blot illustrating the amount of Ephx2 in cortex (CTX) and hippocampus (HIP) of 5xFAD transgenic (Tg) mice and nontransgenic (N-Tg) control mice. β-actin was used as a loading control. (E) Quantification of sEH/β-actin ratio in mouse cortex and hippocampus in the Western blot in panel DF. (F) Quantification of relevant EET and EDP regioisomers (displayed as a percentage of a reference nontransgenic mouse) in 5xFAD transgenic (Tg) and nontransgenic (N-Tg) control mouse brains. The numbers on the x-axis denote carbon numbers where the double bonds were located in the corresponding polyunsaturated fatty acids. Data are means ± SEM of eight to ten human postmortem brain tissue samples per group (A-B, Table S2) or six to eight mice per group of mixed gender (C-F). **P < 0.01, *P < 0.05. Data were analyzed by unpaired Student's *t*-test.

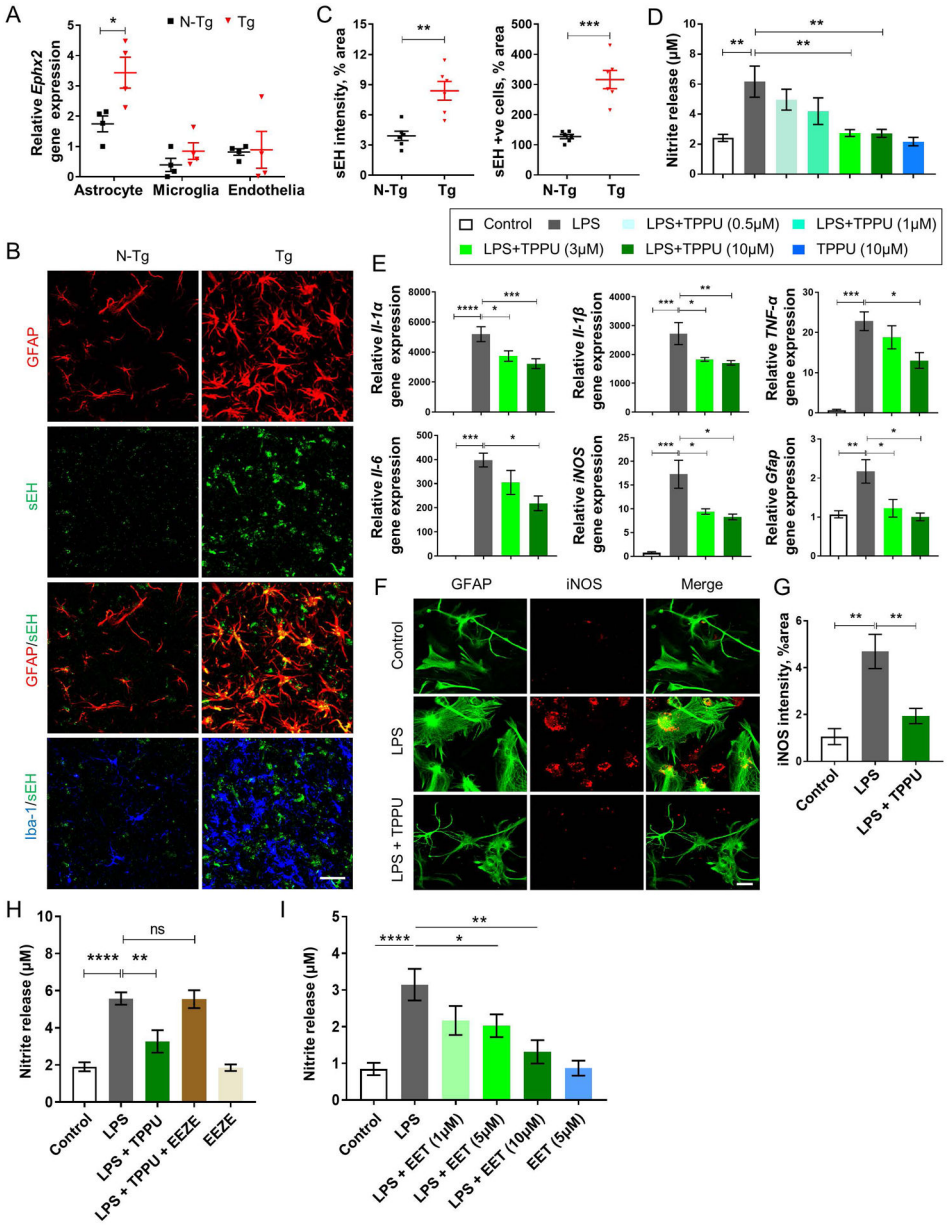

Fig. 2. sEH expression in transgenic and nontransgenic mouse astrocytes before and after LPS treatment.

(A) qPCR analysis of mRNA expression of *Ephx2* in sorted brain astrocytes, microglia and vascular endothelia of 5xFAD transgenic (Tg) mice and nontransgenic (N-Tg) control mice. (B) Immunostaining of GFAP (red), sEH (green) and Iba-1 (blue) in hippocampal sections from 5xFAD transgenic (Tg) and nontransgenic (N-Tg) mice at 4.5 months of age. (C) Quantification of sEH staining intensity (left) and sEH-positive cells (right) in hippocampal sections from animals in panel B. (D-G) Analysis of conditioned medium or cell lysates of mouse primary astrocyte cultures pretreated with different doses of TPPU (from 0.5 μM to 10 μM) for 30 minutes followed by treatment with LPS (100 ng/ml) for 24 hours. (D) Nitrite release measured by the Griess assay into media from cultured mouse primary astrocytes is shown. (E) Shown is qPCR analysis of mRNA expression of *Il-1α*, *Il-1β*, *Tnf-α*, *Il-6*, *iNOS*

and *Gfap*. (F) Immunocytochemistry of GFAP (green) and iNOS (red) expression in cultured mouse primary astrocytes and (G) quantification of iNOS intensity is shown. (H) Nitrite release was measured by the Griess assay in conditioned media from cultured mouse primary astrocytes pretreated with TPPU (10 μM) or the pan-EET receptor antagonist 14,15-EEZE (1 μM) for 30 minutes followed by LPS treatment (100 ng/ml) for 24 hours. (I) Nitrite concentrations in conditioned media from cultured mouse primary astrocytes pretreated with different doses of 11,12-EET (from 1 μM to 10 μM) for 30 minutes followed by LPS treatment (100 ng/ml) for 24 hours are shown. Data are means ± SEM of four to six mice per group of mixed gender (A-C) or three independent experiments (D-I). ****P < 0.0001, ***P < 0.001, **P < 0.01, *P < 0.05; n.s., not significant. Data were analyzed either by unpaired Student's *t*-test (A, C) or by one-way ANOVA with Tukey's multiple comparison test (D, E, G, H, I). Scale bar in (B) is 50 μm and in (F) is 100 μm.

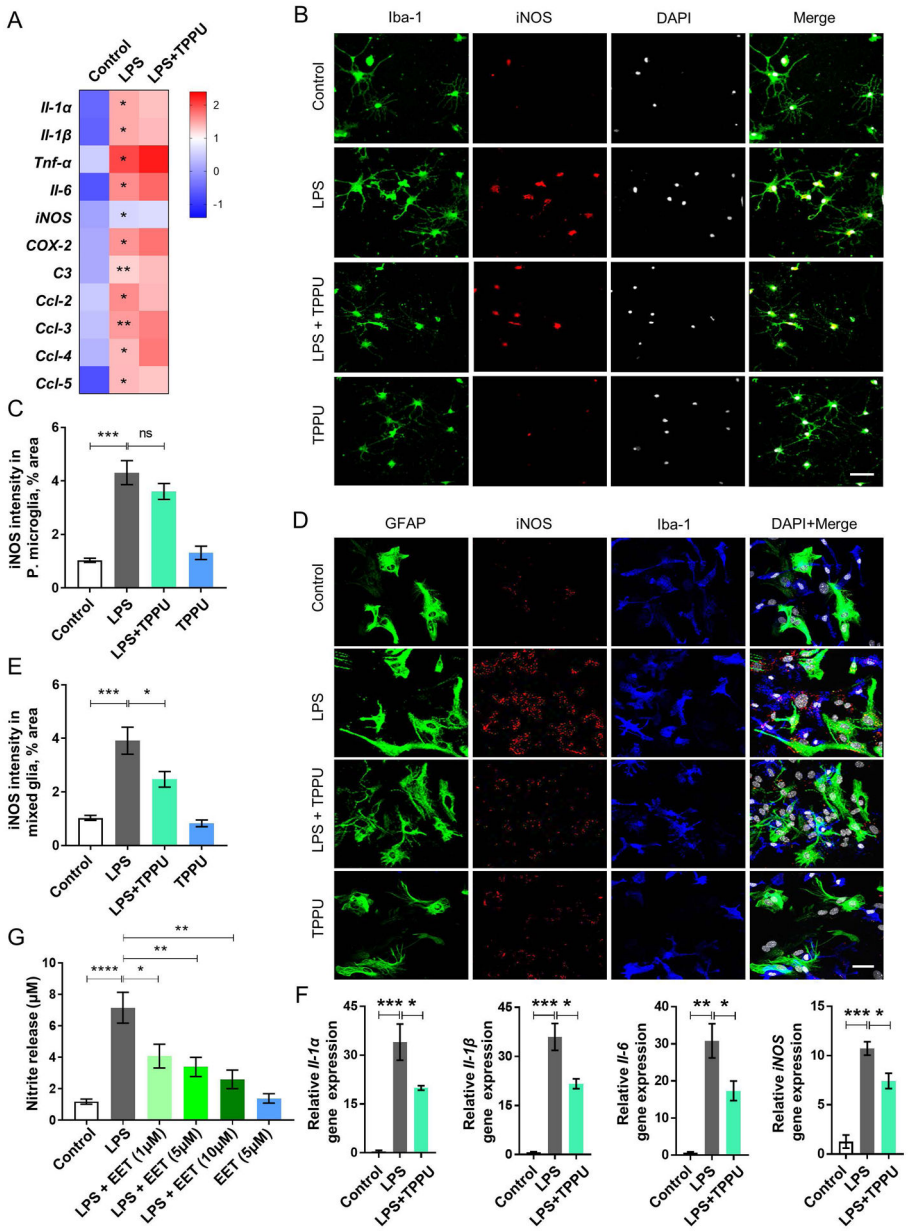

Fig. 3. TPPU and EET suppress microglial reactivity through astrocyte-microglia cross-talk.

(A) Heat map of qPCR analysis of inflammatory gene expression in mouse primary microglia treated with vehicle (control), LPS (100 ng/ml) or LPS with a pre-treatment of 10 μM TPPU (LPS + TPPU). The asterisks in the LPS column represent the comparison between control and LPS. LPS vs. LPS + TPPU: non-significant for all genes. (B) Shown is immunocytochemistry for expression of Iba-1 (green) and iNOS (red) by mouse primary microglia treated with vehicle (control), LPS, LPS + TPPU, or TPPU alone. DAPI stains the nucleus in the merged panel. (C) Quantification of iNOS staining intensity in panel B. (D) Immunofluorescence staining for expression of GFAP (green), iNOS (red) and Iba-1 (blue) in mixed mouse glia cultures treated with vehicle (control), LPS, LPS + TPPU, or TPPU alone. DAPI stains the nucleus in the merged panel. (E) Quantification of iNOS staining

intensity in panel D. (F) qPCR analysis of mRNA expression of *Il-1α*, *Il-1β*, *Il-6* and *iNOS* in mixed mouse glia cultures. (G) Nitrite concentrations measured by the Griess assay in conditioned media from mouse primary microglia cultures are shown. Data are means ± SEM of three independent experiments. ****P < 0.0001, ***P < 0.001, **P < 0.01, *P < 0.05; n.s., not significant. Data were analyzed by one-way ANOVA with Tukey's multiple comparison test. Scale bars, 75 μm.

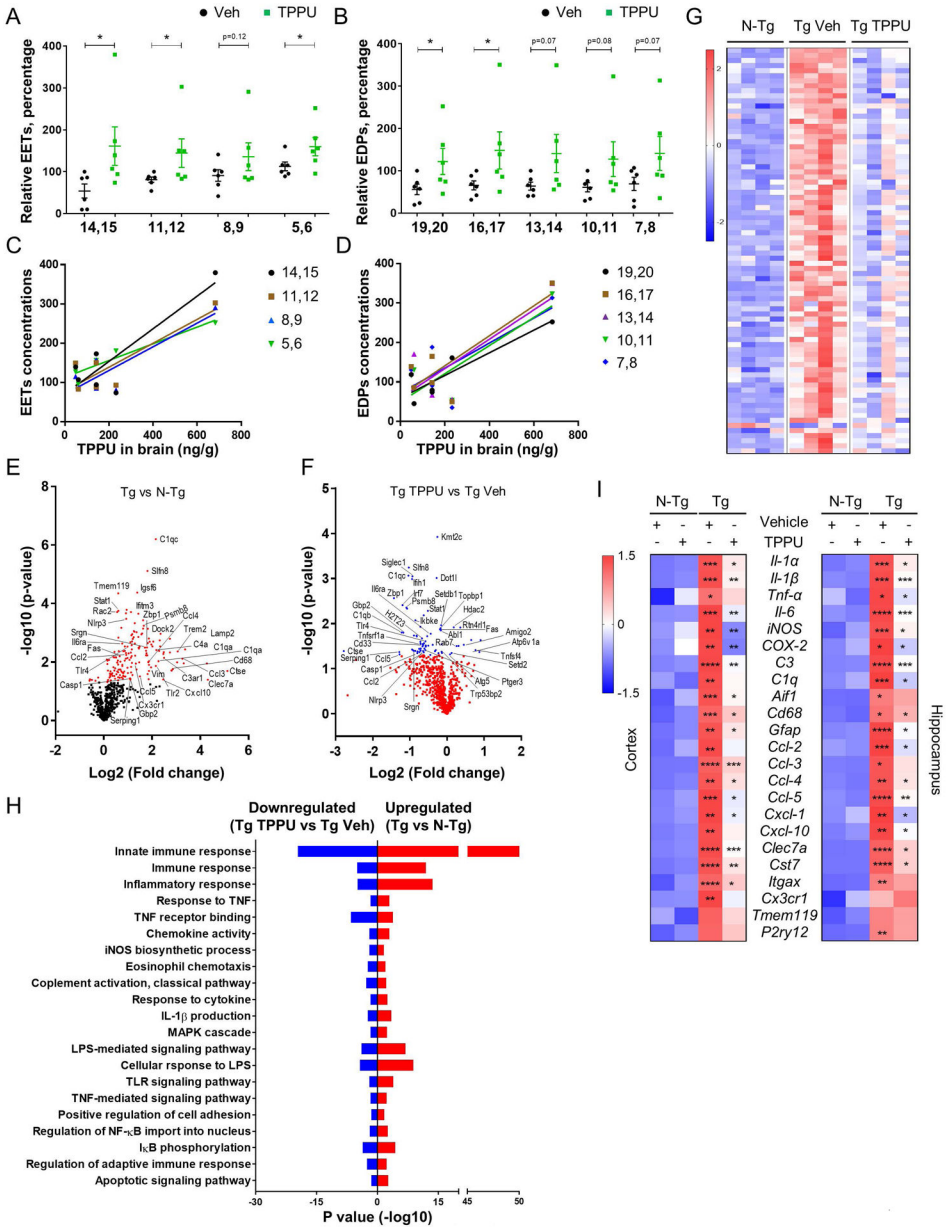

Fig. 4. TPPU engages its target and attenuates inflammatory gene expression in 5xFAD transgenic mouse brains.

(A, B) Quantification of relevant EETs (A) and EDPs (B) in mouse brains from vehicle-treated (Veh) or TPPU-treated 5xFAD transgenic mice (displayed as a percentage of a reference vehicle-treated transgenic mouse). (C) Correlation of brain TPPU concentration with concentrations of different EET regioisomers ($r=0.874$, $p<0.0238$ for 14,15-EET; $r=0.866$, $p<0.026$ for 11,12-EET; $r=0.02$ for 8,9-EET; $r=0.947$, $p<0.004$ for 5,6-EET). (D) Correlation of brain TPPU concentration with concentrations of different EDP regioisomers ($r=0.899$, $p<0.015$ for 19,20-EDP; $r=0.84$, $p<0.037$ for 16,17-EDP; $r=0.796$, $p<0.581$ for 13,14-EDP; $r=0.84$, $p<0.036$ for 10,11-EDP; $r=0.762$, $p<0.079$ for 7,8-EDP). (E, F) Shown is a volcano plot of neuroinflammation gene expression profiles using an Nanostring nCount panel. Differences in gene expression in the hippocampus were stratified as follows: (E)

5xFAD transgenic (Tg) versus nontransgenic (N-Tg) mice, and (F) 5xFAD transgenic (Tg) mice treated with TPPU compared to vehicle (Veh). For each plot, significance is plotted against fold-change (log2 values). Red dots and blue dots denote genes with adjusted significance of $p<0.05$. (G) Shown is a heat map of relative expression of inflammatory pathway genes in nontransgenic (N-Tg) mice and in transgenic (Tg) mice treated with vehicle (Veh) or TPPU. (H) Gene ontology (GO) and pathway analysis of differentially expressed genes in panel G is shown, with identification of significant GO terms (biological processes) associated with differentially expressed genes. The vertical axis represents the GO category, and the horizontal axis represents the P-value (−Log10) of the significant GO terms. Red bars represent significantly upregulated inflammatory pathways in Tg mice vs N-Tg mice, and blue bars represent significantly downregulated inflammatory pathways in transgenic (Tg) mice treated with TPPU versus vehicle (Veh). (I) Heat map shows qPCR analysis of mRNA expression in mouse cortex (left) and hippocampus (right). Asterisks in transgenic (Tg) vehicle (+) TPPU (−) column represent significant changes compared to nontransgenic (N-Tg) vehicle (+) TPPU (−). Asterisks in transgenic (Tg) vehicle (−) TPPU (+) column represent significant changes compared to nontransgenic (N-Tg) vehicle (−) TPPU (+). Data are means ± SEM of either six to eight mice of mixed gender (A-D) or four male only mice (E-H) per group. Data were analyzed by Student's *t*-test (A, B) or by two-way ANOVA with Bonferroni's multiple comparison test (I). For (C) and (D), correlation coefficients (r) were computed using Pearson correlations and each dot represents an individual mouse and linear regression line.

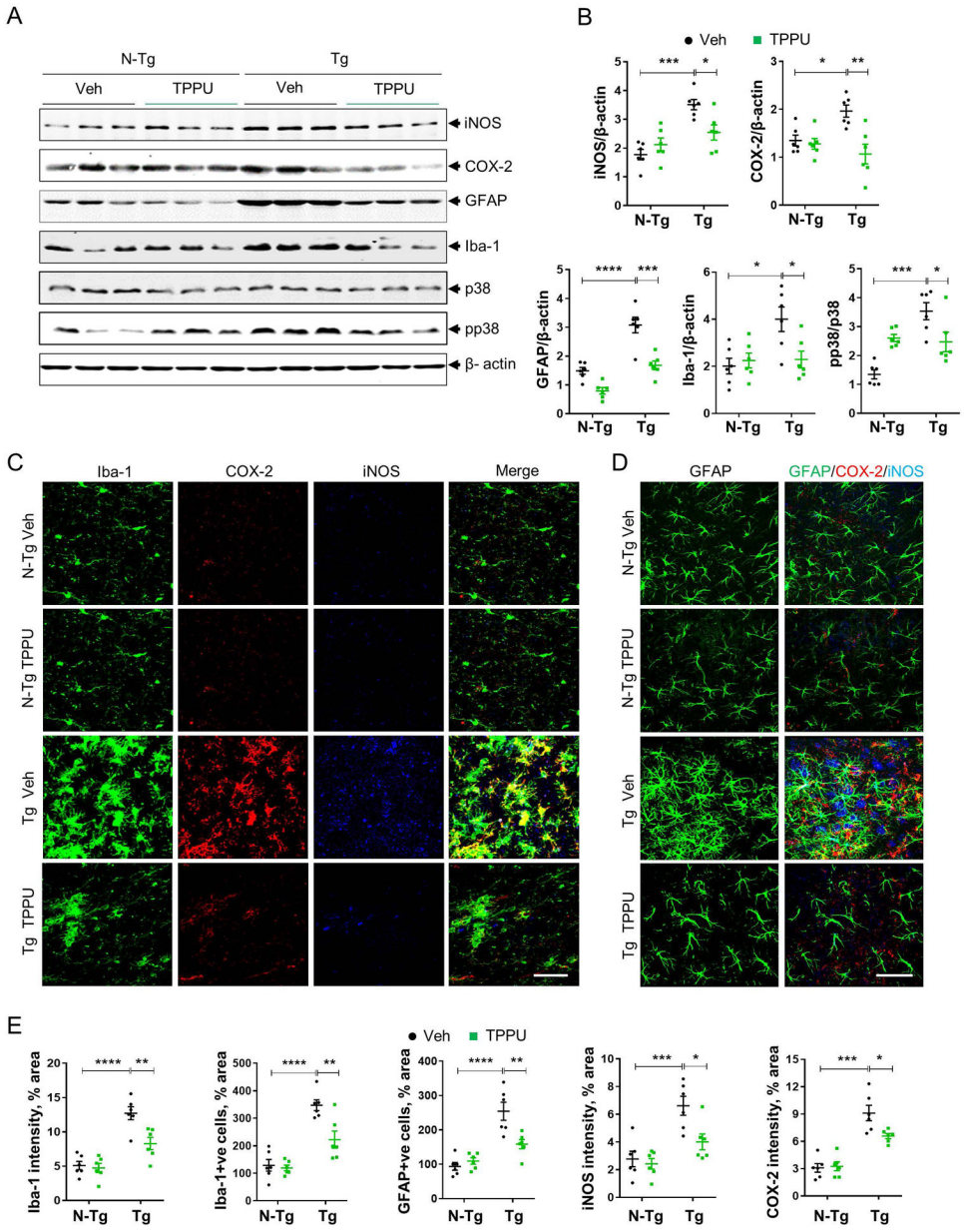

Fig. 5. TPPU reduces neuroinflammatory markers and gliosis in 5xFAD transgenic mouse brains.

(A) Shown is a representative Western blot of expression of iNOS, COX-2, GFAP, Iba-1, total p38 and phosphorylated p38 (pp38) in hippocampal samples from nontransgenic (N-Tg) mice and 5xFAD transgenic (Tg) mice treated with vehicle (Veh) or TPPU starting at 2 months of age for 2.5 months. β-actin was used as a loading control. (B) Quantification of Western blot in panel A. (C) Shown is triple immunofluorescence staining for expression of Iba-1 (green), COX-2 (red) and iNOS (blue) in the hippocampus of nontransgenic (N-Tg) mice and 5xFAD transgenic (Tg) mice treated with vehicle (Veh) or TPPU starting at 2 months of age for 2.5 months. (D) Shown is immunofluorescence staining for GFAP alone (left) and merged panel of GFAP (green), COX-2 (red) and iNOS (blue) staining (right) in the hippocampus of nontransgenic (N-Tg) mice and 5xFAD transgenic (Tg) mice treated

with vehicle (Veh) or TPPU starting at 2 months of age for 2.5 months.. (E) Quantification of Iba-1, iNOS and COX-2 staining intensities and the number of Iba-1-positive and GFAP-positive cells in the hippocampus is sh own. Data are means ± SEM of six to eight mice per group of mixed gender. ****P < 0.0001, ***P < 0.001, **P < 0.01, *P < 0.05. Data were analyzed by two-way ANOVA with Bonferroni's multiple comparison test. Scale bars, 50 μm.

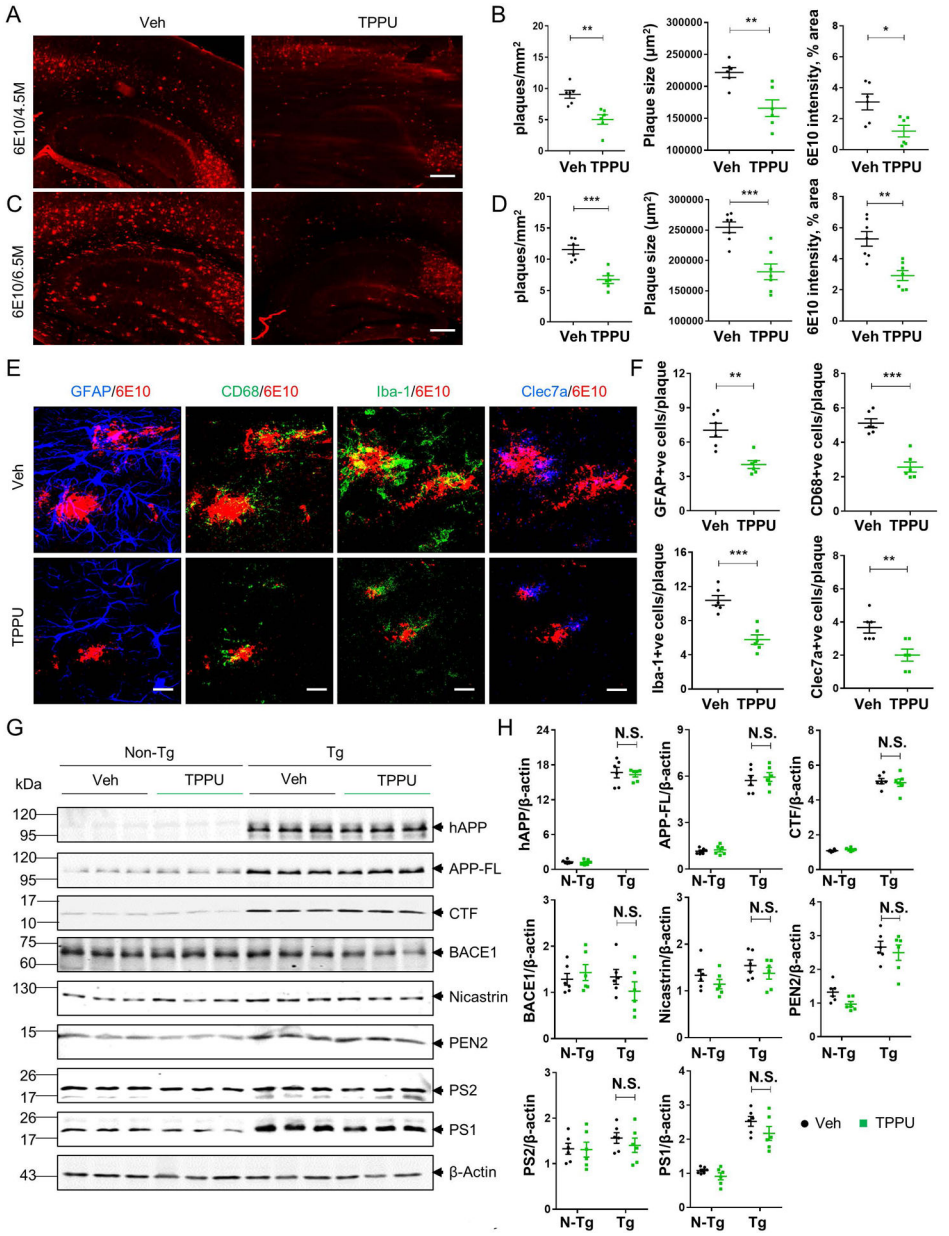

Fig. 6. TPPU reduces Aβ burden but does not alter APP processing in 5xFAD transgenic mouse brains.

(A) Shown is immunohistochemistry with the 6E10 antibody of mouse brains from 4.5 month old 5xFAD transgenic mice treated with vehicle (Veh) or TPPU for 2.5 months. (B) Shown is quantification of amyloid plaques/mm^2 area, amyloid plaque size (μm^2) and 6E10 staining intensity from panel A. (C) Shown is immunohistochemistry with the 6E10 antibody of mouse brains from 6.5 month old 5xFAD transgenic mice treated with vehicle (Veh) or TPPU for 4.5 months. (D) Shown is quantification of amyloid plaques/mm^2 area, amyloid plaque size (μm^2) and 6E10 staining intensity from panel D. (E) Shown are representative double immunofluorescence images of staining in the hippocampus of 4.5 month old 5xFAD transgenic mice treated with vehicle (Veh) or TPPU for: GFAP (blue) and 6E10 antibody (red), CD68 (green) and 6E10 antibody (red), Iba-1 (green) and 6E10

antibody (red) and Clec7a (blue) and 6E10 antibody (red). (F) Shown is quantification of GFAP-positive cells, CD68-positive cells, Iba-1-positive cells and Clec7a-positive cells within a 100 μm radius of an amyloid plaque (86 to 123 plaques per group were counted) from panel E. (G) Shown is a representative Western blot of expression of hAPP, APP-FL, CTF, BACE1, Nicastrin, PEN2, PS2 and PS1 in hippocampal samples from 4.5 month old nontransgenic (N-Tg) and 5xFAD transgenic (Tg) mice treated with vehicle (Veh) or TPPU. β-actin was used as a loading control. (H) Scattered dot plot shows mean protein expression compared to β-actin from data in panel G. Each dot represents normalized protein expression data of a mouse. Data are means ± SEM of six to eight mice per group of mixed gender. ***P <0.001, **P < 0.01, *P < 0.05, N.S., not significant. Data were analyzed by either Student's *t*-test (B, D, F) or by two-way ANOVA with Bonferroni's multiple comparison test (H). Scale bars in (A) and (C), 400 μm and in (E), 100 μm.

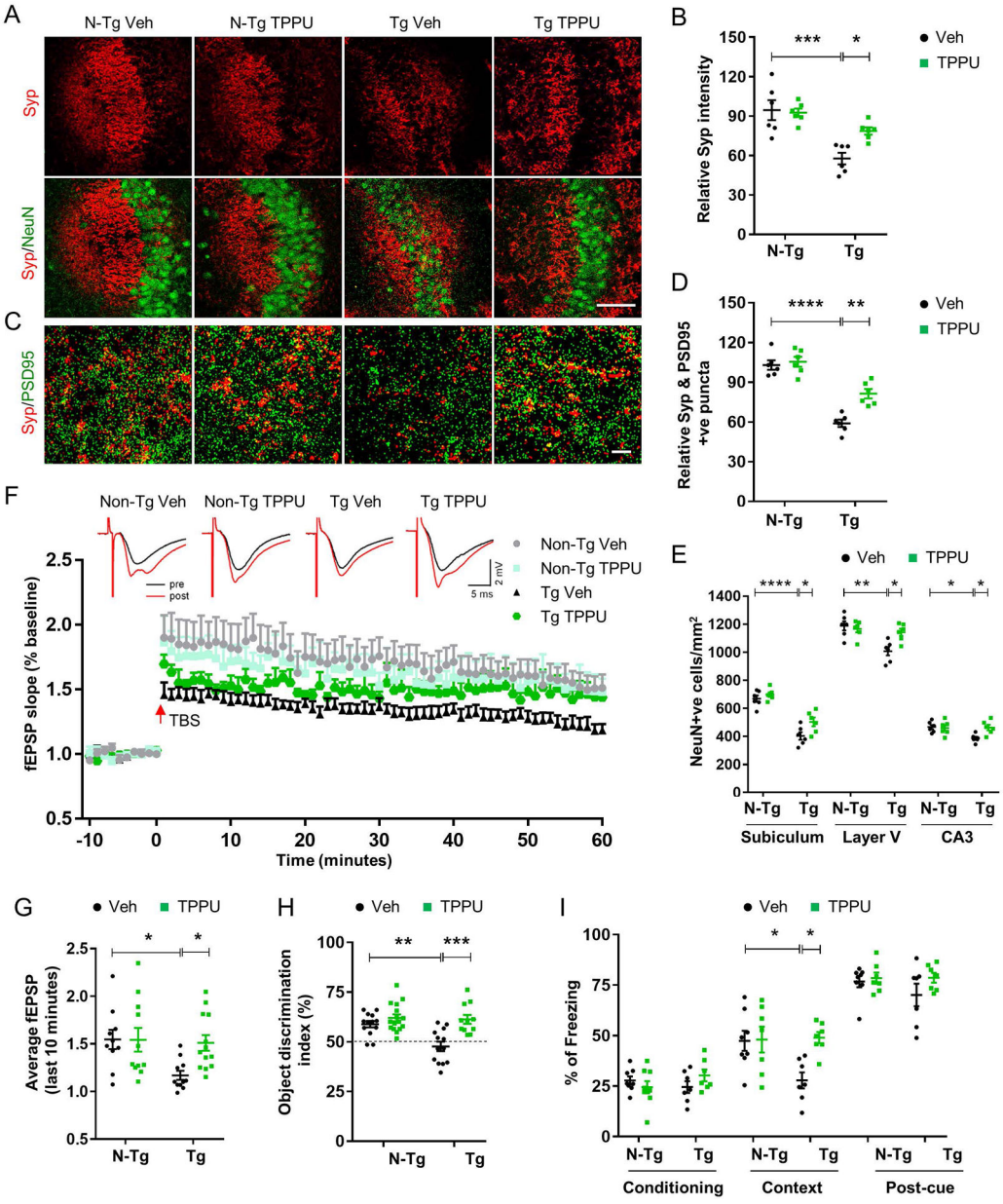

Fig. 7. TPPU ameliorates synaptic deficits and cognitive function in 5xFAD transgenic mice.

(A) Shown are representative images of co-immunostaining for synaptophysin (Syp) and NeuN in hippocampal CA3 sections from 6.5 month old nontransgenic (N-Tg) and 5xFAD transgenic (Tg) mice treated with vehicle (Veh) or TPPU. (B) Shown is quantification of relative synaptophysin (Syp) staining intensity, % area from panel A. (C) Shown are high resolution images of co-immunostaining for synaptophysin (Syp) and PSD95 in hippocampal CA3 sections from 6.5 month old nontransgenic (N-Tg) and 5xFAD transgenic (Tg) mice treated with vehicle (Veh) or TPPU. (D) Shown is quantification of synaptophysin (Syp) and PSD95 staining in double-positive puncta, % of nontransgnic (N-Tg) vehicle (Veh) from panel C. (E) Shown is quantification of NeuN-positive cells in subiculum, layer V of cortex and hippocampal CA3 of 6.5 month old nontransgenic (N-Tg) and 5xFAD

transgenic (Tg) mice treated with vehicle (Veh) or TPPU. (F) Shown is the slope of field excitatory postsynaptic potential (fEPSP) in response to theta burst stimulation delivered to the Schaffer collateral pathway of 6.5 month old nontransgenic (N-Tg) and 5xFAD transgenic (Tg) mice treated with vehicle (Veh) or TPPU. (Top) Shown are fEPSP traces before (black) or after (red) theta burst stimulation. Calibration was 2 mV, 5 ms. (G) Shown is the average fEPSP slope in the last 10 minutes of theta burst stimulation. (H) Shown is the novel object recognition test displayed as the object discrimination index in 4.5 month old nontransgenic (N-Tg) and 5xFAD transgenic (Tg) mice treated with vehicle (Veh) or TPPU for 2.5 months. The dotted line represents a 50% chance of random object exploration. (I) Shown are the results of a fear conditioning test in 4.5 month old nontransgenic (N-Tg) and 5xFAD transgenic (Tg) mice treated with vehicle (Veh) or TPPU for 2.5 months. The percent of mice showing a freezing response is displayed for the conditioning arm (left), contextual arm (center) and post-cued arm (right) of the fear conditioning test. Values are expressed as mean ± SEM of six to nine mice per group (A-E), 10–13 sections from 5–6 animals per group (F, G) or twelve to sixteen mice per group (H, I). All mouse groups were mixed gender. Data were analyzed by two-way ANOVA with Bonferroni's multiple comparison test. ***P < 0.001, **P < 0.01, *P < 0.05. Scale bar in (A), 200 μm and in (C), 30 μm.